




## Using clathrate hydrates for gas storage and gas-mixture separations: experimental and computational studies at multiple length scales

Ioannis N. Tsimpanogiannis, Joseph Costandy, Panagiotis Kastanidis, Sally El Meragawi, Vasileios K. Michalis, Nikolaos I. Papadimitriou, Stylianos N. Karozis, Nikolaos I. Diamantonis, Othonas A. Moulτος, George E. Romanos, Athanassios K. Stubos & Ioannis G. Economou


To cite this article: Ioannis N. Tsimpanogiannis, Joseph Costandy, Panagiotis Kastanidis, Sally El Meragawi, Vasileios K. Michalis, Nikolaos I. Papadimitriou, Stylianos N. Karozis, Nikolaos I. Diamantonis, Othonas A. Moulτος, George E. Romanos, Athanassios K. Stubos & Ioannis G. Economou (2018) Using clathrate hydrates for gas storage and gas-mixture separations: experimental and computational studies at multiple length scales, *Molecular Physics*, 116:15-16, 2041-2060, DOI: [10.1080/00268976.2018.1471224](https://doi.org/10.1080/00268976.2018.1471224)

To link to this article: <https://doi.org/10.1080/00268976.2018.1471224>

 View supplementary material 



 Published online: 15 May 2018.

 Submit your article to this journal 







 Article views: 368

 View related articles 

 View Crossmark data 

 Citing articles: 9 View citing articles 

## Using clathrate hydrates for gas storage and gas-mixture separations: experimental and computational studies at multiple length scales

Ioannis N. Tsimpanogiannis <sup>a</sup>, Joseph Costandy <sup>b\*</sup>, Panagiotis Kastanidis<sup>c</sup>, Sally El Meragawi<sup>b†</sup>, Vasileios K. Michalis <sup>b,c</sup>, Nikolaos I. Papadimitriou<sup>a‡</sup>, Stylianos N. Karozis<sup>a</sup>, Nikolaos I. Diamantonis<sup>b</sup>, Othonas A. Moulτος <sup>d</sup>, George E. Romanos<sup>c</sup>, Athanassios K. Stubos <sup>a</sup> and Ioannis G. Economou <sup>b</sup>

<sup>a</sup>Environmental Research Laboratory, National Center for Scientific Research ‘Demokritos’, Aghia Paraskevi Attikis, Greece; <sup>b</sup>Chemical Engineering Program, Texas A&M University at Qatar, Doha, Qatar; <sup>c</sup>Institute of Nanoscience and Nanotechnology, National Center for Scientific Research ‘Demokritos’, Aghia Paraskevi Attikis, Greece; <sup>d</sup>Engineering Thermodynamics, Process & Energy Department, Faculty of Mechanical, Maritime and Materials Engineering, Delft University of Technology, Delft, Netherlands

### ABSTRACT

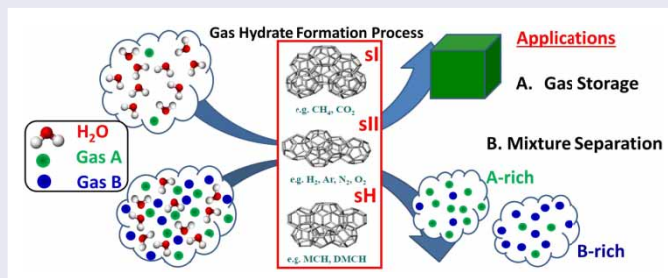
Clathrate hydrates have characteristic properties that render them attractive for a number of industrial applications. Of particular interest are the following two cases: (i) the incorporation of large amounts of gas molecules into the solid structure has resulted in considering hydrates as possible material for the storage/transportation of energy or environmental gases, and (ii) the selective incorporation of guest molecules into the solid structure has resulted in considering hydrates for gas-mixture separations. For the proper design of such industrial applications, it is essential to know accurately a number of thermodynamic, structural and transport properties. Such properties can either be measured experimentally or calculated at different scales that span the molecular scale-up to the continuum scale. By using clathrate hydrates as a particular case study, we demonstrate that performing studies at multiple length scales can be utilised in order to obtain properties that are essential to process design.

### ARTICLE HISTORY

Received 30 December 2017  
Accepted 16 April 2018

### KEYWORDS





Clathrate hydrate; molecular dynamics; grand canonical Monte Carlo; experimental; three-phase equilibria



## 1. Introduction and background

Water molecules under appropriate pressure and temperature conditions (usually high pressures or low temperatures) can self-assemble, and through hydrogen bonding can form a solid, ‘ice-like’, framework that contains cavities (cages) with specific geometry, where guest molecules of appropriate size can be engaged (enclathrated) [1]. The resulting crystalline materials (clathrate hydrates) can be stable under appropriate conditions, with the


weak van der Waals interactions between the water lattice and the engaged guest molecules providing the stability of the material. The crystalline structure can collapse (i.e. a process known as hydrate dissociation) as a result of the absence of the stabilising guest molecules or if it is brought outside the temperature and pressure stability conditions. The most common types of hydrates that have been identified, based on their crystal structure, are sI, sII and sH [1]. Their

**CONTACT** Ioannis N. Tsimpanogiannis  [i.tsimpanogiannis@qatar.tamu.edu](mailto:i.tsimpanogiannis@qatar.tamu.edu)  Environmental Research Laboratory, National Center for Scientific Research ‘Demokritos’, Aghia Paraskevi Attikis 15310, Greece; Ioannis G. Economou  [ioannis.economou@qatar.tamu.edu](mailto:ioannis.economou@qatar.tamu.edu)  Chemical Engineering Program, Texas A&M University at Qatar, Doha PO Box 23874, Qatar

\*Current address: McKetta Department of Chemical Engineering, The University of Texas at Austin, Austin, Texas, 78712, USA.

†Current address: Department of Chemical Engineering, Monash University, Clayton, Victoria 3800, Australia.

‡Public Power Corporation, Testing Research and Standards Center, Leontariou 9, Kantza, 15351 Pallini, Greece.

 Supplemental data for this article can be accessed here. <https://doi.org/10.1080/00268976.2018.1471224>

**Table 1.** Structural properties of hydrates, as used in the GCMC simulations.

	Hydrate structure		
	sI	sII	sH
Molecular formula	25·6L·46H <sub>2</sub> O	16S·8L·136H <sub>2</sub> O	3S·2M·1L·34H <sub>2</sub> O
Cavity types	S: 5 <sup>12</sup> L: 5 <sup>12</sup> 6 <sup>2</sup>	S: 5 <sup>12</sup> L: 5 <sup>12</sup> 6 <sup>4</sup>	S: 5 <sup>12</sup> L: 5 <sup>12</sup> 6 <sup>8</sup> M: 4 <sup>3</sup> 5 <sup>6</sup> 6 <sup>3</sup>
Space group	<i>Pm3n</i>	<i>Fd3m</i>	<i>P6/mmm</i>
Lattice constants (Å)	$a = b = c = 12.03$	$a = b = c = 17.05$	$a = b = 12.21, c = 10.14$
Number of unit cells	$3 \times 3 \times 3$	$2 \times 2 \times 2$	$3 \times 4 \times 3$
Number of H <sub>2</sub> O molecules	1242	1088	1224

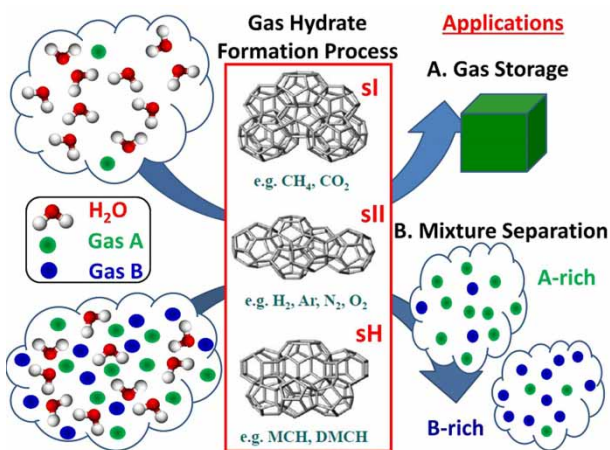
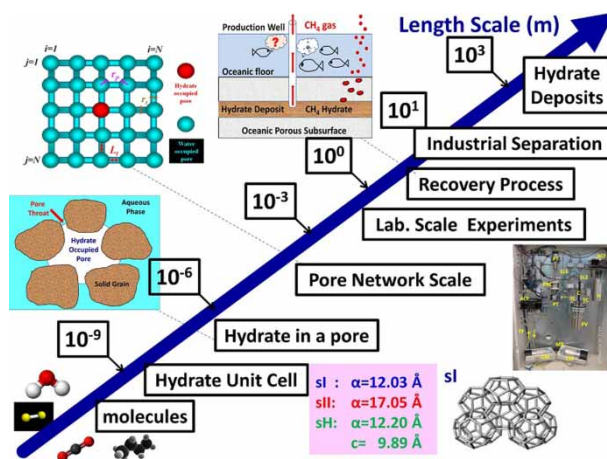
Note: S: small; M: Medium; L: Large.

composition and structural properties are shown in Table 1.

The characteristic behaviour of hydrates to selectively incorporate large amounts of certain guest molecules, from pure gases or gas mixtures, into the three-dimensional cages/cavities has been under consideration for the use of hydrates in a number of important industrial applications, including the storage and transportation of gases, and the separation of mixtures. A characteristic schematic of two processes that are of interest to the current study is shown in Figure 1. In particular, hydrates can be considered as alternative materials for the storage and transportation of ‘energy carrier’ gases, such as CH<sub>4</sub> [2] and H<sub>2</sub> [3,4], or the sequestration of the ‘greenhouse’ gas CO<sub>2</sub> [5]. Furthermore, huge amounts of CH<sub>4</sub> are stored within naturally occurring hydrate deposits (oceanic or permafrost sediments) that could be used as a possible future energy source [6]. On the other hand, separation applications include gas mixtures separation [7–11], natural gas purification [12,13], water desalination [14–16] and waste-water contaminant removal [17]. Exploring the two aforementioned groups of industrial applications is of interest to the current discussion.

For the proper design of such industrial applications, it is essential to know accurately a number of

structural, thermodynamic and transport properties (i.e. lattice constants, three-phase equilibrium conditions, guest gas solubilities, gas-storage capacities, kinetic rates of hydrate formation/dissociation, diffusion coefficients). Such properties can either be measured experimentally or calculated at different length scales, ranging from the molecular up to the continuum scale. As Figure 2 clearly indicates, we can identify different aspects of problems that need to be addressed at length scales that span many orders of magnitude. In particular, while the size of the hydrate unit cell is in the range 1.2–1.7 nm, the size of hydrate deposits can be in the hundreds of metres. An interesting discussion on the issue was presented by Ripmeester [18]. Therefore, depending on the needs and the available resources, one can focus the research interest at different scales such as the atomistic scale (i.e. molecular level), the mesoscale and the field scale (i.e. effective continuum). At the molecular level, approaches such as Molecular Dynamics (MD) and Monte Carlo (MC) simulation can be used for property calculations [19,20]. On the other hand, at the mesoscale, methods that are often encountered include Lattice-Boltzmann (LB) simulations [21], Pore-Network (PN) simulations [22,23] and Dissipative Particle Dynamics (DPD) simulations [24,25]. Finally, at the field scale, one uses effective continuum

**Figure 1.** Schematic of the hydrate-related industrial applications of interest to the current study.**Figure 2.** Schematic of the length scales involved in hydrate-related studies.

descriptions of the momentum, heat and mass balance equations that require a number of thermodynamic and transport properties to be known [26]. Often, properties that are calculated at a particular length scale are transferred for use at a different scale.

The main objective of this work is to demonstrate that calculations and experiments at different length scales can be utilised efficiently to obtain properties that are essential to process design. In the current discussion, we use the example of clathrate hydrates as a particular case study. We report an overview of our recent simulation, computational and experimental multi-scale studies of pure and mixed hydrates [27–47]. At the molecular scale, we have used: (i) MD simulations in order to calculate the three-phase equilibrium conditions (using the phase coexistence methodology [48]) of pure CH<sub>4</sub>, pure CO<sub>2</sub> and binary CH<sub>4</sub> + CO<sub>2</sub> hydrates, as well as structural properties, and the self-diffusion coefficients of hydrate-forming *n*-alkanes in water, (ii) MC simulations to calculate the storage capacities of CH<sub>4</sub> and H<sub>2</sub> hydrates and the gas-mixture separation efficiencies for various hydrate structures. The calculations are compared against experimental measurements from the literature and from a newly designed experimental set-up, as well as continuum-scale calculations using models that couple an Equation of State (i.e. PC-SAFT [49,50]; Peng–Robinson (PR) [51]; Soave–Redlich–Kwong (SRK) [52]) with the van der Waals–Platteeuw statistical theory [53].

While the current study presents an overview of previously reported studies by our research group, it also provides additional comparisons of properties calculated by the different approaches considered, that were not previously reported, as well as some further novel aspects, such as the web-based gas-storage calculator described in Section 3.4.3.

## 2. Methodology

### 2.1. Molecular level simulations

Simulations at the molecular level can provide physical insight based on the interactions between molecules and contribute significantly to the prediction of macroscopic physical properties and to the improvement of the theoretical basis of the macroscopic models (i.e. equations of state).

- (i) Elucidating the hydrate equilibrium behaviour (i.e. three-phase equilibria) is a major issue for the design of a process that is based on hydrates. Experimental work is often costly and takes a significant amount of time. Therefore, molecular simulations, in close

cooperation with macroscopic models can assist significantly in the pre-screening stage of the process design. Once the favourable conditions are identified, then, experiments can be conducted for verification of the results and generate data for the detailed process design. However, the experiments can be kept to a minimum level (reducing, therefore, the cost), since all the unfavourable conditions will have been excluded. An excellent example of such an approach is the work of Frankcombe and Kroes [54], that used MD simulations to calculate the guest-hydrate interaction energies for the small/large cavity occupancies of structures sII, and sH hydrates. The authors considered approximately 50 different guests and concluded that the proposed methodology can be used as a screening approach to identify guests that are worthy of further study. Further studies can be either experimental or macroscopic modelling.

MD simulations can be used for calculating thermodynamic, transport and kinetic properties. In the current work, the following properties were examined:

- Three-phase equilibrium conditions for pure CH<sub>4</sub>[27], CO<sub>2</sub>[28] and the binary CH<sub>4</sub> + CO<sub>2</sub> hydrates [29].
- Solubilities of pure CH<sub>4</sub>[27], CO<sub>2</sub>[28], H<sub>2</sub>S (in progress) and the binary CH<sub>4</sub> + CO<sub>2</sub>[29] mixture in water at two- and three-phase equilibrium conditions.
- Hydrate structural parameters including the isothermal compressibility and the isobaric thermal expansion coefficient for pure CH<sub>4</sub> and CO<sub>2</sub> hydrates [30,31].
- Self-diffusion coefficients of hydrate-forming *n*-alkane gases (C<sub>1</sub> – C<sub>5</sub>) in water [32].

All the aforementioned properties examined during the current research work are of importance to energy-related and environmental applications [1].

- (ii) The accurate determination of the occupancy of each type of hydrate cavity is an issue of crucial importance for the evaluation of the selectivity of hydrates during the separation of a gas mixture [39]. The preferential inclusion in hydrate cavities (under certain temperature, and pressure conditions) of a guest component that is part of a gas mixture increases the selectivity towards the guest. In addition, cavity occupancies are important for the economic evaluation of the gas-storage capacity of hydrates. By increasing or decreasing the cavity occupancy for a specific guest of interest, one



can improve or deteriorate, respectively, the storage capacity of a given hydrate structure. An accurate determination of the gas molecules distribution within the hydrate cavities based on experimental measurements is a demanding and difficult task [55–57]. For this reason, molecular simulations such as Grand Canonical Monte Carlo (GCMC) [58–61] can be used as alternative approaches. CGMC, when assisted with advanced, molecular-based, macroscopic theories that capture accurately the behaviour of fluid and solid phases [62], can have an important contribution towards obtaining the detailed gas distribution within the different cavities during mixture separation, and the estimation of the total gas content. In the current study, extensive MC simulations have been performed in order to assess various aspects of the storage of a number of gases (i.e. Ar [33], H<sub>2</sub>[34,36,37], CH<sub>4</sub>[35,38], CO<sub>2</sub>[39]) that are of industrial interest, including the effect of various force fields and the structural parameters of hydrates. Furthermore, MC simulations have been performed in order to study the separation of the binary CH<sub>4</sub> + CO<sub>2</sub> gas mixture using hydrates [39].

## 2.2. Macroscopic (effective continuum) level simulations

In order to design separation processes such as natural gas purification [12,13] or CO<sub>2</sub> capture from flue-gas streams [9–11], accurate thermodynamic, transport and kinetic properties are required for all the involved pure components and their mixtures. When fluid mixtures are involved, performing experiments that consider all the possible mixture compositions can be costly and time-consuming. Therefore, it is of utmost importance to develop macroscopic-description tools that can calculate the required properties of the pure components and their mixtures. Such models are, for example, the Equations of State (EoS) [63]. A major requirement of such macroscopic tools, in addition to their accuracy, is the computational efficiency. Namely, such tools should be able to produce ‘accurate results, calculated really fast’. Molecular simulations can use very detailed physics; however, they are very computationally demanding, and therefore, the size of the system under consideration has to be relatively small (i.e. in the order of nanometres). Such types of simulations are hard to use in process calculations. On the other hand, an accurate and computationally fast macroscopic model (e.g. EoS-based model) can be used for screening purposes in the optimisation of a given separation process.

Therefore, it is deemed essential to develop such reliable macroscopic tools that can describe accurately the

equilibrium properties of hydrates of gas mixtures. In addition to the accuracy of the model, it is important to incorporate a strong theoretical foundation in the model so that it can be used safely to extrapolate the predictions outside the range used to fit the parameters. To this purpose:

- Cubic (i.e. PR, SRK) and non-cubic (PC-SAFT) EoS were developed for three-phase equilibria calculations [42,44], and solubility calculations under two- [41] or three-phase equilibria [42,44].
- Simple combination models have been evaluated for three-phase equilibria calculations of gas mixture hydrate equilibria [43].

## 2.3. Laboratory experiments

Experimental techniques are valuable tools to calibrate both the microscopic and macroscopic models and to provide accurate data for process design. In particular, the experimental data can be used to optimise the model parameters of the macroscopic models (e.g. EoS for the thermodynamic hydrate equilibrium calculations). In principle, macroscopic models perform well when used for calculations with parameters that are kept within the range of model development. Occasionally, problems can occur when macroscopic models are used for extrapolations outside the range of development. It is therefore essential to identify conditions and perform experiments that will enable the safe extrapolation of the macroscopic models. To this purpose, a novel experimental apparatus was designed, constructed and validated for the measurement of three-phase equilibria and fluid phase analysis [45]. In particular, we measured:

- Hydrate equilibrium conditions for pure CH<sub>4</sub>, CO<sub>2</sub>[45] and binary CH<sub>4</sub> + CO<sub>2</sub> gas [46].
- The corresponding solubility of the two gases in water under two- or three-phase equilibrium conditions [47].

A detailed discussion on experimental methods, as well as experimental measurements, can be found in the book of Sloan and Koh [1].

## 3. Discussion of studies

The work presented here combines computational studies at multiple length scales (i.e. molecular and macroscopic level) with experimental measurements at the laboratory scale, where a novel experimental apparatus was designed, validated and subsequently utilised to measure three-phase equilibrium conditions of pure

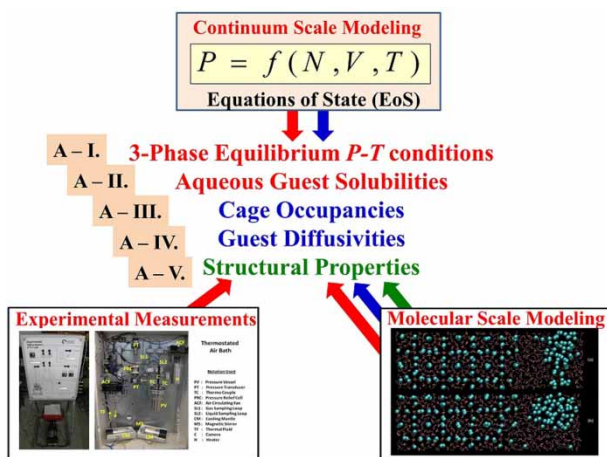


**Figure 3.** Schematic of the properties examined and the approaches used in the current study. Colour code for properties/arrows: Red colour indicates that all three approaches were used; blue colour indicates that only two approaches (i.e. molecular and continuum-level modelling) were used and green colour indicates that only molecular level modelling was used. Additional schematics and details for the experimental approach can be found in Ref. [45,46], while for molecular modelling in Ref. [27–29].

$\text{CH}_4$ ,  $\text{CO}_2$  and binary  $\text{CH}_4 + \text{CO}_2$  hydrates, as well as the corresponding gas solubilities at two- and three-phase equilibrium conditions. Figure 3 shows a detailed schematic of the properties examined along with the calculation approaches used.

At the molecular level, MD simulations were utilised using the open-source package GROMACS [64–66] in order to obtain the three-phase equilibrium conditions, hydrate crystal structural parameters, liquid densities, gas solubilities at three- and two-phase equilibrium conditions and hydrate-former gas self-diffusion coefficients in water. The gas-storage capacity, chemical potential calculations and the gas-mixture separation studies were performed with the GCMC simulation method using the open-source package *MCCCS Towhee* [67]. Our simulations were performed in various statistical ensembles [primarily the isobaric-isothermal (NPT), and the canonical (NVT) ensemble]; systems with 250–5000 molecules were used, depending on the mixture and the property of interest. When possible, systems were tested as to ensure that no system-size dependencies affected the simulation results. All the physical quantities reported were calculated from sufficiently long runs (MD simulations) or after adequate MC steps (MC simulations) in order to ensure relatively low statistical uncertainties.

Calculations at the macroscopic level were performed using either cubic (PR, SRK) or non-cubic (PC-SAFT) EoS with in-house developed codes. Commercial simulators (CSMGem [1]) for hydrate equilibria calculations

were also used. Further details of all the experimental and computational methods employed in this work can be found in the corresponding papers.

### 3.1. Structural properties

Costandy et al. [30] reported extensive MD simulation results of pure  $\text{CH}_4$  and  $\text{CO}_2$  hydrates at a wide range of pressure and temperature conditions focusing on the calculation of the lattice constants (i.e. defined as the length of the edge of the cubic hydrate unit cell) of the two pure hydrates and their dependence on pressure and temperature. The calculated lattice constants were correlated using second-order polynomials which were functions of either temperature or pressure. Finally, the obtained correlations were used in order to calculate two derivative properties, namely the isothermal compressibility, defined as  $\kappa_T = -1/V(\partial V/\partial P)_T$ , and the isobaric thermal expansion coefficient, defined as  $\alpha_P = 1/V(\partial V/\partial T)_P$ , where  $V$  is the calculated volume of the hydrate unit cell. The MD simulation results were also compared with reported experimental measurements and other simulation studies and good agreement was found for the case of isothermal compressibility. It should be noted that the isothermal compressibility,  $\kappa_T$  (i.e. particularly the inverse compressibility known as bulk modulus) of hydrates is a parameter encountered during the interpretation of seismic data obtained from the geophysical surveys used to identify natural hydrate deposits [68,69]. This parameter is a good example of the interplay between calculations at different length scales. While the initial MD calculations are performed at a length scale of a few nanometres (i.e. the unit cell of sI hydrates has a lattice constant equal to  $1.203 \times 10^{-9}\text{m}$ ; see also Table 1 for the lattice constants of the other hydrate structures), subsequently, the calculated parameters are used for calculations at a length scale of metres or hundreds of metres (i.e. natural hydrate deposits). The particular range spans approximately 10–12 orders of magnitude, which is essentially almost the entire span shown in Figure 2.

On the other hand, for the case of isobaric thermal expansion coefficient, good agreement was found only with other simulation studies, while the simulation studies were in disagreement with experiments, especially at low temperatures. This is an inherent deficiency of popular water models such as TIP4P/Ice [70], and TIP4P/2005 [71].

Costandy et al. [31] subsequently presented a detailed discussion on the issue, and introduced a simple methodology to rectify the specific problem. The proposed correction was based on observations reported previously by Conde et al. [72]. These authors compared quantum

path-integral (PI) simulations of the empty hydrate structures (i.e. sI, sII and sH) that were performed using the TIP4PQ/2005 [73] model for water, with classical MD simulations using the same model. They observed that nuclear quantum effects can have a significant influence on densities and other properties, especially for temperatures below 150 K. On the other hand, for temperatures above 150 K, hydrates can be modelled using classical simulations provided that an effective potential is used. In their study, Conde et al. [72] observed that the densities of the pure hydrates obtained from the classical simulations using the TIP4PQ/2005 [73] force field are about  $0.03 \text{ g/cm}^3$  higher than those obtained from the quantum PI simulations, while having an increasing trend at lower temperatures. The particular difference was utilised by Costandy et al. [31] to introduce the correction as follows: Once the lattice constant,  $a$ , for a hydrate unit cell becomes available from classical MD simulations (CS) the hydrate density,  $\rho_{\text{Hyd}}^{(\text{CS})}$ , could be calculated [1] through:

$$\rho_{\text{Hyd}}^{(\text{CS})} = \frac{n_w \text{MW}_w + \sum_i^2 \theta_i v_i \text{MW}_g}{N_{Av} V_{\text{cell}}^{(\text{CS})}}, \quad (1)$$

where  $n_w$  is the number of water molecules per hydrate unit cell,  $\text{MW}$  is the molecular weight of water ( $w$ ) and guest gas ( $g$ ),  $N_{Av}$  is the Avogadro's number,  $\theta_i$  is the fractional occupancy of cavity  $i$  by the gas guest ( $\theta_i = 1$ , for the case of 100% occupancy – fully occupied cavities),  $v_i$  is the number of type  $i$  cavities per water molecule in the unit cell, and  $V_{\text{cell}}^{(\text{CS})} = a^3$  is the hydrate unit cell volume. Subsequently, the hydrate density could be corrected through the following equation:  $\rho_{\text{Hyd}}^{\text{corr}} = \rho_{\text{Hyd}}^{(\text{CS})} - C$ , where  $C$  is a correction function and superscript 'corr' denotes the corrected value. Costandy et al. [31] considered two cases: (i)  $C$  is constant ( $C \approx 0.03 \text{ g/cm}^3$  [72]), and (ii)  $C$  is a function of temperature ( $C(T) = \rho_{\text{empty}}^{(\text{CS})} - \rho_{\text{empty}}^{(\text{PI})}$ ). The study of Costandy et al. [31] is based on the inherent assumption that in the absence of any available quantum PI simulation data for partial/fully occupied hydrates, similar corrections to the case of the empty hydrates could be applied. Such an approach resulted in obtaining a methodology with generalised applicability.

The temperature dependence for case (ii) was obtained by fitting the density difference data of Conde et al. [72] for the empty sI hydrate in the temperature range 77–125 K to a second-degree polynomial. Therefore, one can substitute in Equation (1) the obtained value for  $\rho_{\text{Hyd}}^{\text{corr}}$  and re-solve it in order to calculate the corrected value for the lattice constant:  $a^{\text{corr}} = (V_{\text{cell}}^{\text{corr}})^{1/3}$ . Costandy et al. [31] reported that the use of a constant  $C$  improved the

calculation of the lattice parameters; however, it still can't capture the correct behaviour at low  $T$ 's. On the other hand, the use of a variable correction  $C$  significantly improved the calculation of the lattice constants even at very low  $T$ 's.

The methodology of Costandy et al. [31] was initially developed and found to perform well for cases of sI hydrates with single cage occupancies and for guests without strong nuclear quantum effects (i.e. methane, carbon dioxide). Subsequently, the particular methodology was tested for the case of propane and tetrahydrofuran (THF) sII hydrates by Fang et al. [74] and found to produce very good results for the calculated lattice constants at low  $T$ 's, confirming the generalised applicability of the methodology of Costandy et al. [31].

### 3.2. Three-phase equilibrium studies

#### 3.2.1. Molecular level

Several studies [27–29] were performed in order to calculate the three-phase equilibrium condition using the phase coexistence methodology [48]. In the particular methodology, different phases including a solid hydrate, liquid water and the guest gas (i.e. pure gases:  $\text{CH}_4$ ,  $\text{CO}_2$ ,  $\text{H}_2\text{S}$ ; or the mixture  $\text{CH}_4 + \text{CO}_2$ ) are brought in contact and through MD NPT simulations, the system is allowed to evolve to the equilibrium state that corresponds to the given conditions. The three-phase configuration, used in the series of studies, consisted of a solid hydrate slab, two liquid water slabs surrounding the hydrate slab and one guest gas slab which lies between the water slabs. Therefore, a total of four slabs were placed in the following arrangement: solid hydrate (H) – liquid water (W) – gas (G) – liquid water (W), denoted as a (HWGW) configuration. Figure 4 shows a schematic representation of the phase coexistence methodology used for the three-phase equilibrium calculations. A brief description of the methodology is provided for completeness. By performing a temperature scan (for a constant given pressure), it is possible to determine the three-phase coexistence temperature as follows: For a given pressure and temperature, long MD simulations were performed (in the  $NPT$  ensemble) and the total potential energy of the system was monitored closely. An overall increase in the total potential energy indicates hydrate dissociation, while an overall decrease in the total potential energy indicates hydrate growth. For a given pressure, the value of the three-phase equilibrium temperature was estimated as the average of the highest temperature at which hydrate growth occurs and the lowest temperature at which hydrate dissociation occurs. In order to account for the stochastic behaviour of the system (i.e. when close to the equilibrium temperature the system can



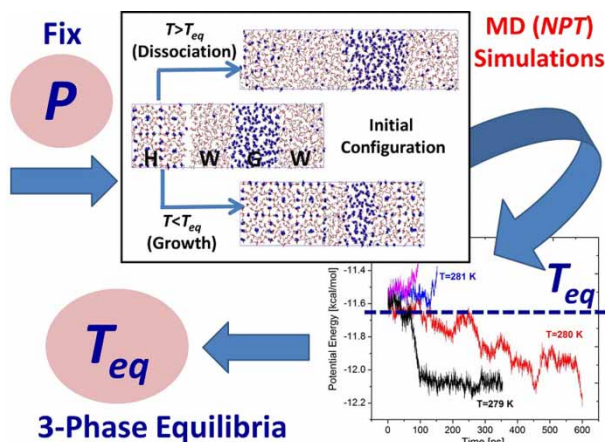


**Figure 4.** A schematic depiction of the phase coexistence methodology used for the three-phase equilibrium calculations [27–29].

either evolve towards hydrate growth or hydrate dissociation), multiple realisations were considered that resulted from using different initial velocities for the molecules in the system [27].

Figure 5 is a ‘Pressure vs. Temperature’ plot comparing the MD results with the three-phase coexistence curves as predicted from CSMGem (denoted with lines). The comparison includes the cases of pure CO<sub>2</sub> hydrate (black diamonds), pure CH<sub>4</sub> hydrate (green circles) and mixed

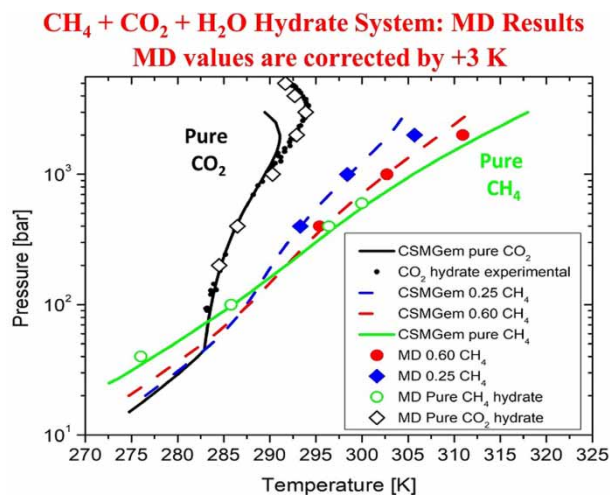


**Figure 5.** Pressure vs. Temperature at three-phase equilibrium conditions for the system CH<sub>4</sub> + CO<sub>2</sub> + H<sub>2</sub>O. Comparison of MD results (CO<sub>2</sub>: black diamonds [28]; CH<sub>4</sub>: green circles [27]; CH<sub>4</sub> + CO<sub>2</sub>: blue diamonds, red circles [29]) with the three-phase coexistence curves as predicted with CSMGem (denoted with lines). Solid lines correspond to pure hydrates while dashed lines to mixed hydrates of various gas bulk composition. Small black circles correspond to carbon dioxide hydrate experimental data [1].

CH<sub>4</sub> + CO<sub>2</sub> hydrates at two different gas bulk compositions (blue diamonds and red circles). For this particular comparison, the MD results are corrected by +3 K in order to account for the fact that TIP4P/Ice water model is known to under-predict the melting point of hexagonal ice I<sub>h</sub> by approximately 3 K [75]. We can observe very good agreement between the corrected MD results and the experimental measurements, as well as the macroscopic simulations with the exception of the higher pressures considered for the case of pure CO<sub>2</sub> hydrate. In order to obtain such good agreement between experiments and MD simulations for gases like CH<sub>4</sub>, CO<sub>2</sub> or their mixtures, our recent studies identified that the following requirements should be met during the simulations:

- Multiple simulation runs should be performed at each pressure and temperature in order to account for the stochastic nature of the process.
- A water model that describes accurately the melting point of hexagonal ice, I<sub>h</sub>, is essential. This requirement was previously reported by Conde and Vega [76], who then suggested the use of the TIP4P/Ice water model. All of our recent studies have also confirmed the particular finding of Conde and Vega. Moreover, this is supported by the findings of Miguez et al. [77] for CO<sub>2</sub> hydrate, and Yagasaki et al. [78] for ethylene oxide (EO) and THF hydrates. Both studies used the MD-based phase coexistence methodology.
- The accurate description of gas solubility in the aqueous phase is also required. For the case of pure CH<sub>4</sub> hydrate, the use of a model such as the OPLS-UA [79] (i.e. a single-interaction site that interacts *via* a 12–6 Lennard–Jones (LJ) potential; united-atom approach) is adequate since the CH<sub>4</sub> solubility in water can be accurately described [80]. On the other hand, for the case of pure CO<sub>2</sub> or CO<sub>2</sub>-containing mixtures, the TraPPE [81] force field is not capable of predicting accurately the CO<sub>2</sub> solubility in water, a fact also reflected in the accuracy of the three-phase equilibria using the phase coexistence methodology. To address the issue, Costandy et al. [28] recommended that all the cross interaction parameters between water and CO<sub>2</sub> should be calculated with the classical Lorentz–Berthelot (LB) combining rules [19,20], with the exception of the cross interaction energy parameter between the oxygen in water and the oxygen in CO<sub>2</sub> ( $\epsilon_{O(CO_2)-O(H_2O)}$ ). A modification factor,  $\chi$ , was used to correct the LB cross interaction energy parameter according to the equation:  $\epsilon_{O(CO_2)-O(H_2O)} = \chi \sqrt{\epsilon_{O(CO_2)} \epsilon_{O(H_2O)}}$ , where  $\epsilon_{O(CO_2)}$  and  $\epsilon_{O(H_2O)}$  are the LJ energy parameters for oxygen in CO<sub>2</sub> and water, respectively. This modification was



subsequently used in the study of Waage et al. [82], who considered a MC simulation-based approach to calculate the three-phase equilibrium conditions for CO<sub>2</sub> hydrate. This study clearly demonstrated that the use of the modification introduced by Costandy et al. [28], when coupled with the use of the TIP4P/Ice water model, improved significantly the calculated three-phase equilibrium conditions. Therefore, the study of Waage et al. [82]: (i) confirmed the validity of the modification for the LB cross interaction energy parameter, and (ii) confirmed the finding of Conde and Vega [76], regarding the need to use the TIP4P/Ice water for accurate phase equilibria calculations of hydrates.

- On the other hand, preliminary results (i.e. work currently in progress in our research group) for H<sub>2</sub>S have indicated that even though the above requirements are met, there are no accurate H<sub>2</sub>S force fields for hydrate equilibrium calculations using the phase coexistence approach.

The study of the three-phase equilibria for the ternary system CH<sub>4</sub> + CO<sub>2</sub> + H<sub>2</sub>O is an excellent example demonstrating the use of multi-scale studies in order to fill the missing gaps in the data required for process design. In particular, molecular level methodologies can be calibrated appropriately at conditions where experimental data are available (i.e. at low/high pressures for pure CH<sub>4</sub> and CO<sub>2</sub> hydrates, and at low pressures for mixed CH<sub>4</sub> + CO<sub>2</sub> hydrates) and subsequently use the calibrated models to produce MD simulation data for mixed hydrates at high pressures, where no experimental data are available.

Additional studies of the three-phase equilibrium conditions using MD-based approaches, with a varying degree of success, include among others studies reported in Ref. [83–87].

### 3.2.2. Macroscopic level

The most common theoretical tool for the study of clathrate hydrate equilibrium is a theory based on Statistical Mechanics that has been developed initially by van der Waals and Platteeuw (vdWP) [53] and subsequently modified by other workers [88–106]. Modifications were introduced in order to relax some of the original limitations (i.e. hydrate lattice distortion [98–100], interactions between the guest molecules and water molecules that are further away than the first shell [101–104], multiple occupancy [95–97], etc.). In the vdWP theory, the chemical potential of water in the hydrate can be expressed as a function of the hydrate cavity occupancies (i.e. fraction of occupied cavities by guest molecules). Therefore, the stability region of the material can be determined because

the formation or dissociation of hydrates is a phase equilibrium process between the hydrate and the aqueous solution (liquid or solid) of the guest gases.

Following Tsimpanogiannis et al. [41], the three-phase equilibria between the hydrate phase (denoted with superscript *H*), the vapour phase (denoted with superscript *V*) and the aqueous phase (denoted with superscript  $\pi$ ), require the following conditions to be satisfied for the temperature, *T*, pressure, *P* and the chemical potential of each component in all phases (subscript *W* denotes water and *g* denotes the hydrate-former guest).

$$T^H = T^\pi = T^V, \quad (2a)$$

$$P^H = P^\pi = P^V, \quad (2b)$$

$$\mu_W^H = \mu_W^\pi = \mu_W^V, \quad (2c)$$

$$\mu_g^H = \mu_g^\pi = \mu_g^V, \quad (2d)$$

The aqueous phase can be either liquid water (for temperatures above 273.15 K) or ice (for temperatures below 273.15 K, for the case of pure water), denoted with superscripts *L* or  $\alpha$ , respectively. Following the notation of Parrish and Prausnitz [88] and Holder et al. [107], the ice water phase is known also as the  $\alpha$ -phase, while the liquid water phase as the *L*-phase.

In order to proceed with the calculation of the chemical potentials, a reference state is required. The most common reference state, that is used for the calculation of the chemical potential of water in the hydrate, is the hypothetical empty hydrate lattice (i.e. no cages occupied by the guest molecules) [53,107]. The empty hydrate lattice is denoted as the  $\beta$ -phase and is a metastable phase. According to the vdWP theory:

$$\frac{\Delta\mu_W^H}{RT} = \frac{\mu_W^\beta - \mu_W^H}{RT} = - \sum_i \nu_i \ln \left( 1 - \sum_j \theta_{ij} \right), \quad (3)$$

where  $\mu_W^\beta$  is the chemical potential of water in the hypothetical empty hydrate lattice, *R* is the gas constant,  $\nu_i$  is the number of cavities of type *i* per water molecule and  $\theta_{ij}$  is the occupancy of the cavity of type *i* by the guest component *j*. Index *j* can be equal to one (case of pure hydrate), two (case of binary hydrate) or higher (case of mixed hydrates). Index *i* takes the values *i* = *S*, *L* for structure sI and sII hydrates and *i* = *S*, *L*, *M* for structure sH hydrates, where *S*, *L* and *M* denote small, large and medium cavities, respectively. The occupancy  $\theta_{ij}$  is

given by a Langmuir-type function of the gas fugacity:

$$\theta_{ij} = \frac{C_{ij}f_j}{1 + \sum_j C_{ij}f_j} \quad (4)$$

where  $C_{ij}$  is the Langmuir constant of the guest component  $j$  in the cavity  $i$  and  $f_j$  is the fugacity of component  $j$ , and can be calculated with an appropriate EoS.

By assuming that the cavity is perfectly spherical and that the water molecules, which form the cavity, are smeared evenly over the surface of the sphere [107], then the Langmuir constants can be calculated from the following simplified configurational integral:

$$C_{ij} = \frac{4\pi}{k_B T} \int_0^\infty \exp\left(-\frac{W(r)}{k_B T}\right) r^2 dr, \quad (5)$$

where  $k_B$  is the Boltzmann constant, and  $W(r)$  is the smoothed-cell potential function along the cavity radius due to the interactions between the guest molecule and the cavity. This potential is derived from the summation of the pair-potentials between the guest molecule and each one of the water molecules of the cavity. Usually, the Kihara hard-core spherical potential is used for the water-guest interactions and is given as a function of the energy well depth,  $\varepsilon$ , the collision diameter for the interaction between the gas and the water molecules (i.e. the distance between the centres of the two molecules when  $U(r) = 0$ ),  $\sigma$ , and the radius of the hard core (i.e. the radial separation at which the guest-water pair potential becomes infinite),  $\alpha$ . Traditionally, the parameters  $\sigma$  and  $\varepsilon$ , are fitted to hydrate equilibrium data in order to have an adequate accuracy to the hydrate equilibrium calculations. A detailed discussion of the various forms of the Kihara potential can be found in the studies of Bakker et al. [105] and Bakker [106].

To simplify the calculations, namely, in order to avoid performing the numerical integration of the complicated expressions given by Equation (5), the Langmuir constants can be considered as temperature-dependent and thus described by:

$$C_{ij} = \left(\frac{A_{ij}}{T}\right) \exp\left(\frac{B_{ij}}{T}\right), \quad (6)$$

where the constants  $A_{ij}$  and  $B_{ij}$  are component- and cavity-specific, and are calculated by fitting hydrate equilibrium experimental data. As a result, instead of using  $\sigma$  and  $\varepsilon$  as the fitting parameters, we use  $A_{ij}$  and  $B_{ij}$  for each cavity type. Consequently, we need to fit four parameters for hydrates of structure sI and sII (while six parameters for structure sH), instead of two parameters if we calculate the Langmuir constants through Equation (5).

This approach, of using Equation (6), was introduced by Parrish and Prausnitz [88].

The right-hand side (RHS) of Equation (2c) can be calculated based on classical thermodynamics, taking again the empty hydrate lattice ( $\beta$ -phase) as the reference state. This is traditionally done following the technique that was originally developed by Parrish and Prausnitz [88], and subsequently simplified by Holder et al. [89]. The popular approach of Holder et al. [89] is given as follows, for the case that liquid water is present in the system ( $T > 273.15\text{K}$ ). In case there is ice present in the system ( $T \leq 273.15\text{K}$ ), Equation (2c) still holds; however, the superscript ( $\beta - L$ ) should be replaced by ( $\beta - \alpha$ ). According to the analysis that was presented by Holder et al. [89] the RHS of Equation (2c) can be calculated as:

$$\begin{aligned} \frac{\Delta\mu_W^L}{RT} &= \frac{\mu_W^\beta - \mu_W^L}{RT} = \frac{\Delta\mu_W^0(T_0, 0)}{RT_0} \\ &\quad - \int_{T_0}^T \frac{\Delta h_w^{\beta-L}(T)}{RT^2} dT + \int_{P_0}^P \frac{\Delta v_w^{\beta-L}}{RT} dP - \ln(a_w), \end{aligned} \quad (7)$$

where  $\Delta\mu_W^0(T_0, 0)$  is the chemical potential difference between water in the pure  $\alpha$ -phase (ice) and water in the empty hydrate (metastable  $\beta$ -phase), at the reference conditions  $T_0$  and  $P_0$  (usually taken to be  $T_0 = 273.15\text{K}$  and  $P_0 = 0.0\text{MPa}$ ).  $\Delta\mu_W^0(T_0, 0)$  is an experimentally determined quantity [108]. The second and third terms on the RHS of Equation (7) describe the temperature and pressure dependence of the chemical potential, respectively, while in the third term,  $\Delta v_w^{\beta-L}$ , is the difference of molar volume between empty hydrate and pure liquid water at temperature  $T$ . The last term is the water activity which is important only for the cases of high solubility of the hydrate-former guest in the aqueous phase. A detailed discussion on how the particular terms can be calculated can be found in the literature [1,41,88,107], while a recent review of modelling approaches is provided by Khan et al. [109].

Following such an approach, El Meragawi et al. [44] examined the three-phase equilibrium pressures of nine pure hydrate components ( $\text{CH}_4$ ,  $\text{C}_2\text{H}_6$ ,  $\text{C}_3\text{H}_8$ ,  $i\text{-C}_4\text{H}_{10}$ ,  $\text{CO}_2$ ,  $\text{N}_2$ ,  $\text{Ar}$ ,  $\text{O}_2$  and  $\text{H}_2\text{S}$ ), along with several typical binary, ternary and quaternary mixtures of them. They considered two EoS, namely, a cubic (PR [31]) and a non-cubic (PC-SAFT [49,50]) coupled with the vdWP theory [53]. In an effort to improve the accuracy of the calculations, the Kihara  $\varepsilon$  parameter has been optimised using hydrate equilibrium experimental data for the pure components. Subsequently, the optimised values have been used for the calculation of the mixtures. Reasonable

agreement between the experimental and calculated values was obtained for the case of the mixtures, given the large sensitivity of the results on the modified parameters. Additional details and discussion can be found in Ref. [44].

Tsimpanogiannis et al. [42] reported an extensive series of thermodynamic calculations using continuum-level modelling based on the coupling of the SRK cubic EoS [52] with the vdWP theory [53] for a number of gases of industrial interest. The authors examined the effect of deviations from the classical LB combining rules primarily on the cavity occupancy of hydrates. They also examined the effect of deviations from the classical LB combining rules on the calculation of the hydrate equilibrium pressure. The following general conclusions were obtained:

- A very strong sensitivity to deviations from the LB reference case on the hydrate equilibrium pressure was identified, while the sensitivity on the cavity occupancies was weaker. Furthermore, the effect on small cavity occupancies was stronger, compared to the case of large cavities.
- In all cases, optimal values for Kihara parameters, capable of producing accurate calculations for the hydrate equilibrium pressures can be found. However, that fact cannot guarantee the accurate calculation of cavity occupancies or the identification of the correct hydrate structure formed.
- Classical vdWP-type models need to be reformulated in order to account for the possibility of multiple cavity occupancy. For example, for the case of N<sub>2</sub> hydrate, experimental measurements have shown that multiple occupancy occurs. Yet, optimal values for Kihara parameters can be found in the literature that produces accurate calculations for the hydrate equilibrium pressures, while predicting single occupancies.
- For accurate predictions of the hydrate equilibrium pressures the consistent/systematic use of: (i) model parameters, and (ii) optimised Kihara parameters, are required. In case of extrapolating outside the range of model development, significant increase in errors can occur, particularly for the case of hydrate equilibrium pressures, while the problem is less serious for cavity occupancies.

### 3.2.3. Laboratory level

Kastanidis et al. [45] designed, constructed and validated a novel experimental apparatus that was used for the measurement of three-phase equilibria and fluid phase analysis. A picture of the apparatus can be seen in the lower left part of Figure 3, while all the design details can be found in Ref. [45,46]. Initially, the experimental

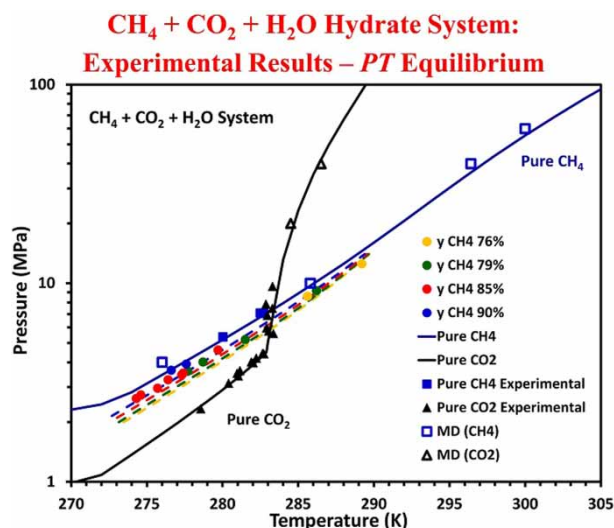


**Figure 6.** Pressure vs. Temperature at three-phase equilibrium conditions for the system CH<sub>4</sub> + CO<sub>2</sub> + H<sub>2</sub>O. Comparison between experimental data (denoted with filled symbols) [45,46], and MD simulations (denoted with empty symbols) [27,28], with calculations using CSMGem [1]. Squares denote data for pure CH<sub>4</sub> hydrates [45], triangles data for pure CO<sub>2</sub> hydrates [45] and circles denote data for the mixed hydrate [46]. Symbols and lines of same colour correspond to same vapour mixture composition.

apparatus was used to measure hydrate equilibrium conditions for pure CH<sub>4</sub> and CO<sub>2</sub> hydrates [45] and subsequently, hydrate equilibrium conditions for the binary CH<sub>4</sub> + CO<sub>2</sub> gas mixture [46]. Figure 6 shows a comprehensive comparison of the experimental measurements obtained within the current work, with the MD simulations (corrected by +3 K, as discussed previously in Section 3.2.1) obtained from the current project at lower pressures [27,28] and EoS–vdWP-based macroscopic simulations.

### 3.2.4. Perspective on phase equilibria calculations

Among the three different approaches that are discussed in the current study for phase equilibria calculations (i.e. atomistic level, macroscopic level and experimental measurements), the macroscopic level approach is the fastest. However, when performing calculations at the macroscopic level, care should be taken when extrapolating the calculations outside the range of the experimental data used for obtaining the fitted parameters (i.e. the Kihara parameters or the *A*'s and *B*'s of Equation (6)) that are involved in the vdWP-based methodology. In the absence of experimental data for a particular system and conditions of interest, one could use results obtained from atomistic level simulations (i.e. 'pseudo-experimental' data). Such simulations require the prior calibration of the interaction potentials used with available experimental data at different conditions.



Once atomistic level simulations are available for the conditions of interest, the particular data can be used in order to re-evaluate the Kihara parameters (or the  $A$ 's and  $B$ 's of Equation (6)) that are involved in the vdWP-based methodology. Following such an approach can result in extending significantly the range of applicability of the vdWP-based methodology. The use of 'computationally-based experimental data' is limited mainly by the available computational power, since such calculations are computationally expensive. The aforementioned conclusions are also applicable for the case of gas solubilities that are discussed in the following section.

### 3.3. Gas solubility studies

#### 3.3.1. Molecular level

As discussed previously in Section 3.2.1., the accurate description of the guest gas solubility in the aqueous phase is one of the requirements for the accurate prediction of the three-phase equilibria using the phase coexistence methodology. Therefore, a limited number of MD simulations were performed in order to explore the accuracy of guest gas solubilities in water (modelled with the TIP4P/Ice) when using the OPLS-UA model for  $\text{CH}_4$  (Michalis et al. [27]), and the modifications to the LB rules for the case of  $\text{CO}_2$  as proposed by Costandy et al. [28]. Both model combinations resulted in accurate guest solubility calculations. Subsequently, the particular model combinations were examined for the ternary system  $\text{CH}_4 + \text{CO}_2 + \text{H}_2\text{O}$  by Michalis et al. [29]. Initial calculations reported by Michalis et al. [29] focused on a comparison with the experimental solubilities in the aqueous phase of the VLE ternary system at 100 bar and 323.15 K reported by Al Ghafri et al. [110]. The particular pressure and temperature experimental conditions were the closest available to the hydrate equilibrium conditions of interest. A comparison between the MD results with the experimental measurement by Al Ghafri et al. [110] showed satisfactory agreement. Therefore, the combination of the particular force fields was confirmed to be adequate to predict correctly the solubilities of both gases in the aqueous phase close to the hydrate equilibrium conditions. Michalis et al. [29] also reported that the solubility of each guest decreases by the addition of the other guest, a conclusion which is in disagreement with the conclusions drawn by Qin et al. [111] and Al Ghafri et al. [110].

Exploring further that particular disagreement was the motivation behind the subsequent work by Kastanidis et al. [47], who reported additional MD simulations, as well as experimental measurements at 100 bar and 323.15 K. Figure 7 shows a comparison between the available MD simulations [29,47] and the new experimental

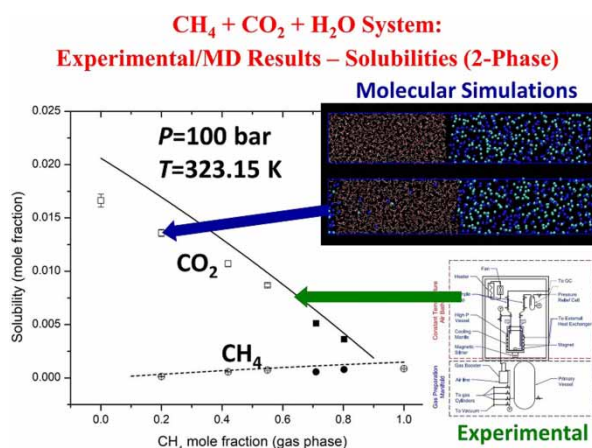


**Figure 7.** Solubilities of  $\text{CO}_2$  (denoted with squares) and  $\text{CH}_4$  (denoted with circles) in the aqueous phase as a function of the  $\text{CH}_4$  composition in the gas phase, at 100 bar and 323.15 K. Comparison of the MD-calculated values (empty black symbols are MD simulations by Michalis et al. [27] and solid black symbols are by Kastanidis et al. [47]) with experimental measurements by Kastanidis et al. [47]. Lines show second-degree polynomial fits of the experimental measurements.

measurements [47]. Additional new MD simulations were also reported exploring higher pressures and temperatures. The work of Kastanidis et al. [47] further confirmed the conclusion by Michalis et al. [29].

#### 3.3.2. Macroscopic level

Tsimpanogiannis et al. [41] provided a detailed review and discussion of both experimental and computational studies examining the solubility of gases of industrial interest under two-phase (H- $L_w$ ) equilibria. In addition, recent studies exploring the particular issues include references [112,113].

Tsimpanogiannis et al. [41] calculated the solubility of  $\text{CH}_4$  in pure water, under three-phase (H- $L_w$ -V), or two-phase (H- $L_w$ ) equilibria using macroscopic theoretical models that were based on the coupling of EoS with the vdWP statistical theory for hydrate equilibria. The authors reported, after comparing with all available experimental data, good agreement between experimental and calculated values, considering the low values for the solubility of  $\text{CH}_4$  in the aqueous phase. From the analysis, it was found that at a constant temperature, the solubility of  $\text{CH}_4$  in the aqueous phase decreases as the pressure increases (such behaviour is in contrast to the trends of experimental observations and calculations for the case under V-L conditions). At the same time, under H- $L_w$  conditions, the hydrate cavity occupancies increase, as the pressure increases. Namely, there is a transfer of  $\text{CH}_4$  from the aqueous liquid phase to the solid hydrate phase as pressure rises.



### 3.3.3. Laboratory level

The experimental apparatus developed by Kastanidis et al. [45–47] was also used in order to measure the solubility of the hydrate-forming guest gases in water under two- or three-phase equilibrium conditions. Figure 8 shows the CO<sub>2</sub> guest solubility in H<sub>2</sub>O as a function of pressure under three-phase equilibrium conditions. Figure 8 shows a comparison between experimental data (denoted with symbols) with calculations using CSMGem [1] and good agreement is observed. On the other hand, Figure 9 shows the hydrate-forming guest (CH<sub>4</sub> or CO<sub>2</sub>) solubility in H<sub>2</sub>O as a function of pressure under two-phase equilibrium conditions that are close to the three-phase equilibrium line. The particular set of experimental measurements is obtained following the three-phase solubility measurements. Namely, after a liquid sample is removed from the high-pressure cell for the three-phase solubility measurement, the pressure drops at a point that corresponds to two-phase equilibrium conditions. Once again, good agreement is observed.

### 3.4. Gas-storage capacity studies

When clathrate hydrates are examined as ‘gas-storage’ materials for industrial gases such as CH<sub>4</sub>, H<sub>2</sub> and CO<sub>2</sub> the following three questions become important and need further exploration: (i) How much gas can be stored in the hydrate structure (i.e. what is the storage capacity of the hydrate structure)? (ii) How much the

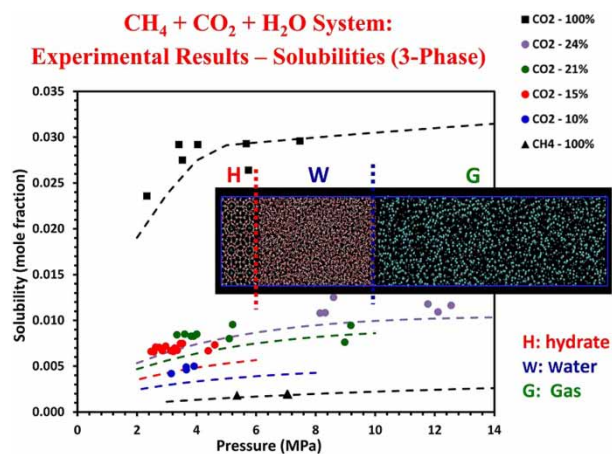


**Figure 8.** Hydrate-forming guest solubility in H<sub>2</sub>O vs. pressure under three-phase equilibrium conditions. Comparison between experimental data (denoted with symbols) with calculations using CSMGem [1]. Triangles denote data for pure CH<sub>4</sub> hydrates [45], squares data for pure CO<sub>2</sub> hydrates [45] and circles denote the CO<sub>2</sub> solubility for the mixed hydrate at different bulk gas composition [46]. Symbols and lines of same colour correspond to same vapour mixture composition.

### CH<sub>4</sub> + CO<sub>2</sub> + H<sub>2</sub>O System: Experimental Results – Solubilities (2-Phase)

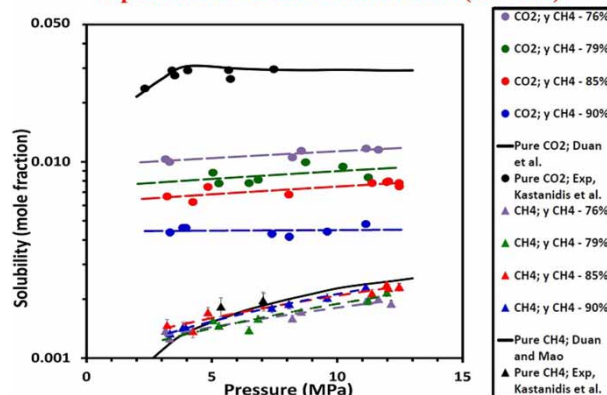


**Figure 9.** Gas (circles denote CO<sub>2</sub> and triangles denote CH<sub>4</sub>) solubility in H<sub>2</sub>O vs. pressure under two-phase equilibrium conditions (close to the three-phase equilibrium line). Experimental data for the pure gases are from Ref. [45], while for the gas mixture from Ref. [46]. The solid line indicating the solubility of pure CO<sub>2</sub> is from Duan et al. [114], while the solid line indicating the solubility of pure CH<sub>4</sub> is from Duan and Mao [15].

storage capacity is affected by the use of hydrate promoters (i.e. components that are used in order to facilitate hydrate formation at more favourable conditions, namely, at higher temperatures or lower pressures)? (iii) What can be done in order to increase the storage capacity of a given hydrate structure?

Such questions have been addressed by the current study, primarily by the use of molecular level studies (GCMC approach), and secondarily by macroscopic models. The determination of the distribution of the guest gas molecules within the hydrate cavities based on experimental measurements requires further attention [55–57] and was not considered in the current work.

GCMC simulations have been extensively used in order to estimate the gas content adsorbed in a porous material. Similarly, the formation of hydrates can be simulated as a process of gas adsorption in a porous solid, where the ‘ice-like’ water framework is considered the porous medium, which is further stabilised by the enclathration of the gas molecules. GCMC simulations can be used in calculating the probability density of finding a hydrate-forming guest molecule within the cages. A typical example is shown in Figure 10 where the probability density of finding a CH<sub>4</sub> molecule (denoted as a cyan circle) inside two large cages (5<sup>12</sup>6<sup>2</sup>) of sI CH<sub>4</sub> hydrate is depicted. Red areas represent high probability and blue areas low probability.

The particular methodology has been used to study the storage capacity within different hydrate structures of various hydrate-forming guests of industrial interest.

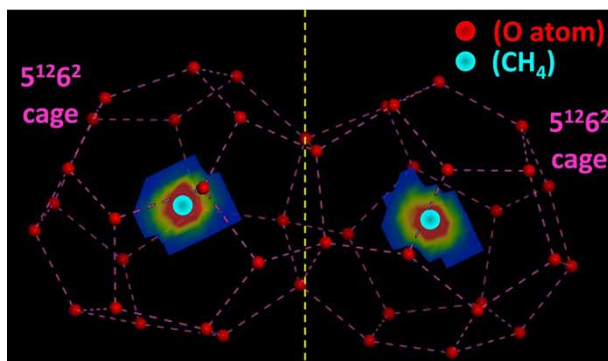


**Figure 10.** Visualisation of a GCMC simulation of CH<sub>4</sub> hydrate. Probability density of finding a CH<sub>4</sub> molecule (denoted as cyan circle) inside two large cages ( $5^{12}6^2$ ) of sI CH<sub>4</sub> hydrate. Red areas represent high probability and blue areas low probability.

A detailed review of MC studies considering hydrates has been presented recently by Tsimpanogiannis and Economou [40].

### 3.4.1. Storage capacity calculations

Probably, the most studied hydrate-forming guests during the recent years are CH<sub>4</sub> and H<sub>2</sub>. Papadimitriou et al. used GCMC simulations to examine the CH<sub>4</sub> storage capacity of sI hydrates [35], and subsequently extended the study to sII and sH hydrates [38]. The obtained cage occupancies were correlated using generalised Langmuir-type expressions. The particular approach was essential in order to account for the multiple occupancy occurring at the  $5^{12}6^8$  cages (i.e. large cages) of the sH hydrates. All other cages of the three most common CH<sub>4</sub> hydrate structures considered (i.e. sI, sII and sH) exhibited single occupancies even at pressures as high as 200 MPa. Such macroscopic expressions are essential for the development of the web-based storage capacity calculator to be discussed in Section 3.4.3.

The authors followed a more refined approach compared to earlier studies. In particular, the pressure and chemical potential were associated using an additional MC simulation at the NVT ensemble using the Widom insertion method [115], while earlier studies used an EoS for the particular calculation (i.e. see also the recent review [40]). An extensive comparison with available experimental data and other computational studies can be found in the corresponding works [35,38].

While the CH<sub>4</sub>-related MC studies by Papadimitriou et al. [35,38] used the TIP4P/Ice water model, as recommended by the MD studies [27,76], the effect of different force fields was examined for the case of H<sub>2</sub> hydrates by Papadimitriou et al. [37]. It was observed in the particular study that the cage occupancies are not very sensitive to the water force field. Therefore, instead of TIP4P/Ice,

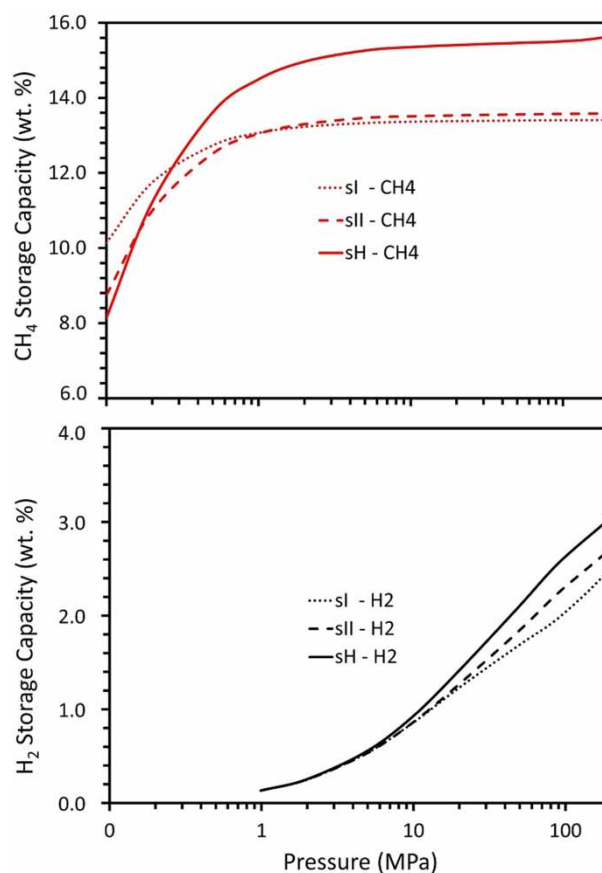


**Figure 11.** Storage capacity of CH<sub>4</sub> (top) and H<sub>2</sub> (bottom) pure hydrates as a function of pressure. Comparison of the storage capacity of the three hydrate structures (sI, sII, and sH) at 250 K, using the TIP4P/Ice [70] water model, the OPLS-UA [79] CH<sub>4</sub> model, and the Silvera-Goldman [117] H<sub>2</sub> model for the calculations.

simpler water models (i.e. SPC/E [116]) were adequate. It should be noted, however, that when the gas-mixture separation is examined with GCMC simulations the results depend strongly on the force field used as was demonstrated in Ref. [39].

Figure 11 shows a comparison of the storage capacity of CH<sub>4</sub> and H<sub>2</sub> pure hydrates. The particular comparison is at 250 K, using the TIP4P/Ice [70] water model, the OPLS-UA [79] CH<sub>4</sub> model and the Silvera-Goldman [117] H<sub>2</sub> model for the calculations.

### 3.4.2. Methods to increase storage capacity

Increasing the gas-storage capacity within a hydrate structure can be the result of a number of factors including the following:

- For all hydrate structures at a constant pressure, lowering the temperature of the hydrate system can result in higher storage capacity.

- For all hydrate structures at a constant temperature, increasing the pressure of the hydrate system can result in higher storage capacity.
- For the case of H<sub>2</sub> or CH<sub>4</sub> hydrates and a fixed temperature and pressure, the storage capacity of the three most common hydrate structures is as follows: sH > sII > sI. This is a direct result of the sizes of the cavities that are present in the hydrate structures.
- Multiple occupancy (i.e. more than one guest molecule in the same cage) can result in increasing the storage capacity. The particular aspect applies to a limited number of small-sized hydrate-forming guests with the most notable case being the H<sub>2</sub> hydrates. For the case of H<sub>2</sub> hydrates, multiple occupancy is observed for all three common hydrate structures. Other guests with the possibility of multiple occupancy include N<sub>2</sub>, O<sub>2</sub>, Ar and CH<sub>4</sub> (applicable only for the large cages of sH structure). Multiple occupancy has been confirmed only for the large cages.
- The use of different hydrate promoters can result in an increase in the lattice constant. This issue, however, is counter-balanced by the fact that the use of promoter reduces the overall storage capacity, since the promoter occupies a fraction of the hydrate cavities.
- Hydrate tuning, has been identified as a possible approach that can result in increased gas-storage capacity. The method was initially explored for the case of binary H<sub>2</sub> + THF sII hydrates. Lee et al. [118] found experimental evidence that under certain THF concentrations there exists a possibility that the hydrate can be stable even when only a fraction of the large cages (5<sup>12</sup>6<sup>4</sup>) is occupied by THF, while the remaining fraction of large cages is occupied by H<sub>2</sub>. As a result of the difficulties in reproducing the particular experimental results, a significant amount of discussion is available in the literature [4,40,119–121]. Subsequent studies [122,123] examined also the case of tuning in the CH<sub>4</sub> + THF hydrate.

All published MC studies of gas-storage in hydrates (see also the recent detailed review [40]) are in good agreement regarding the effect of temperature and pressure on the hydrate storage capacity. In a recent study, Koh et al. [124] reported experimental measurements for the lattice constants of binary sII hydrate systems (H<sub>2</sub> + promoter) where they clearly observed that the size of the promoter used has an effect on the measured hydrate lattice constants. In particular, they examined THF, propane and isobutene as a promoter and reported the lattice constant to be equal to: 17.130, 17.210 and 17.047 Å, respectively. If we consider as the reference case pure H<sub>2</sub> hydrate (which has a lattice constant equal to

17.047 Å [3]) results to an increase of the hydrate unit cell in the range 0.49–1.47%. Sloan and Koh [1] provided an extensive list of experimental measurements for the lattice constants and their variations due to pressure/temperature conditions or guest molecules.

The effect of the change on the lattice constant on the H<sub>2</sub> content of the hydrate for various pressures was examined by Papadimitriou et al. [34,36] using MC studies. The effect was further quantified and is shown in Figure 12 where the % deviation in H<sub>2</sub> storage capacity is plotted as a function of the % deviation in the lattice constant (with respect to the reference case). The particular study utilised the conclusion (i.e. regarding the range of lattice constant values) reported by the MD study of Costandy et al. [30] in order to explore the upper limits of the % change in the lattice constant. Costandy et al. provided a detailed discussion on the effect of temperature and pressure on the hydrate lattice. It should be noted that since hydrates were intended for gas-storage applications, cases of reduced (with respect to the reference case) lattice constant were not considered since they would have resulted in lower storage capacities.

Additional GCMC studies considering the effect of deviations from the classical LB combining rules on the cavity occupancy (which can be translated to storage capacity) have been reported by Papadimitriou et al. [33]. The authors considered argon as the hydrate-forming guest and examined the three most common hydrate structures, since it is known that argon can go through hydrate structural transitions. Significant effects, and the corresponding conditions required, on the storage capacity were identified and reported.

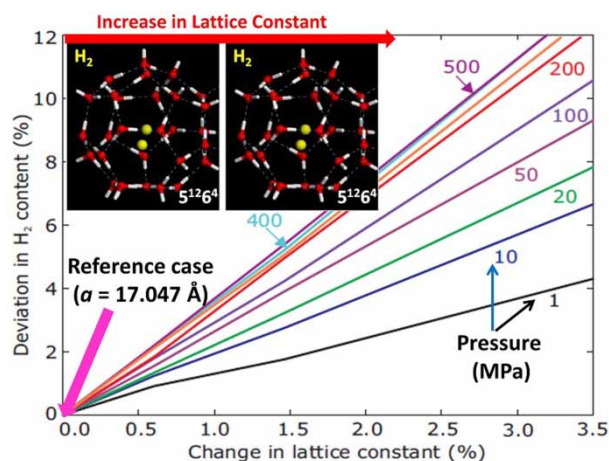


**Figure 12.** Effect of the change in the lattice constant on the H<sub>2</sub> content of the hydrate for various pressures. The inset at the top-left part of the figure shows a single large cage (5<sup>12</sup>6<sup>2</sup>) of sII hydrate with two (left snapshot) or five (right snapshot) H<sub>2</sub> molecules.



### 3.4.3. Web-based gas-storage calculator

A web-based, user-friendly, computational tool was developed that allows calculation of the CH<sub>4</sub> storage capacity of the three most common clathrate hydrate structures. The developed performance assessment tool (PAT) utilised a continuum-level description of an extensive series of MC atomistic-level simulations of CH<sub>4</sub> hydrate cavity occupancies obtained in two recent studies by Papadimitriou et al. [35,38]. The authors examined pressures in the range (1–200 MPa) and three temperature values (i.e. 200, 250 and 300 K) in order to be able to correlate the GCMC calculations for the cage occupancies using generalised Langmuir-type analytical curves. Extended details on the particular simulations are presented in Ref. [35,38]. Essentially, a multi-scale (i.e. molecular and continuum) analysis was performed. A number of different cases are currently available examining the effect of pressure, temperature, hydrate structure and the presence of promoters with different molecular weight. The tool can be used for engineering-type calculations during the preliminary design of processes related to storage and transportation of CH<sub>4</sub>. The storage capacity calculated by the current tool corresponds to the ‘material-based’ capacity accounting only for materials storing CH<sub>4</sub>, as opposed to the case of ‘system-based’ capacity accounting for the tank, valves, piping, etc., as well. A web-based tool was developed utilising the aforementioned mathematical expressions in order to perform parametric calculations. The web-based calculator was named **CH<sub>4</sub>HydPAT** and can be found at the following web-address: <http://www2.ipta.demokritos.gr/CH4HydPAT>

The development of the **CH<sub>4</sub>HydPAT** platform consisted of two parts. The first part was the ‘on the fly’ calculations, according to the user parameterisation. This part was developed with the PHP programming language [125], a well-established method for on-line calculations. The second was the visualisation of the results. It was based on Google Visualisation API [126] which was used for the creation of the charts. The HTML programming language [127] was the cell in which PHP and Google API collaborate [128]. The following five cases of storing CH<sub>4</sub> in solid clathrate hydrates are currently available:

- Pure CH<sub>4</sub> hydrates.
- Binary hydrates with the promoter in the large (*L*) cages.
- Binary hydrates with the promoter in the medium (*M*) cages (applicable only for the case of sH hydrates).
- Binary hydrates with the tuning [118–123] of the promoter in large cages.



**Figure 13.** Snapshot of the third page of the web-based calculator. Example of results (given as a figure and tabulated) for case A with option of examining the comparison of the three structures. Parameters used: pure CH<sub>4</sub> hydrate at  $T = 270$  K.

- Binary hydrates with the tuning of the promoter in medium cages (applicable only for the case of sH hydrates).

Figure 13 provides a snapshot of the results (third page of the web-based calculator depicting the calculated data for an example of case A (i.e. the case of comparing all the three hydrate structures). Additional results and discussion can be found in the Supplemental Information.

### 3.4.4. Perspective on gas storage in hydrates

A detailed discussion on the use of hydrates for H<sub>2</sub> storage can be found in the review of Veluswamy et al. [4], while CH<sub>4</sub> storage in hydrates has been discussed extensively by Veluswamy et al. [129]. The use of clathrate hydrates as gas-storage materials has a number of advantages which make hydrate attractive for industrial applications. In particular:

- Hydrate formation/dissociation requires relatively simple industrial equipment, reducing thus the total capital and operational cost that is associated with the related industrial processes.
- Moderate pressure and temperature conditions are required for hydrate formation. While this is true for the case of pure CH<sub>4</sub> hydrate, higher pressures are required for the case of pure H<sub>2</sub> hydrates. The use of



promoters (i.e. THF) can reduce the required pressure for the mixed ( $\text{H}_2 + \text{Promoter}$ ) hydrate. Promoters, however, can result in storage capacity reduction.

- The gas that is stored in the hydrate phase remains in the molecular form, without any chemical reactions involved. Therefore, complete recovery (100%) of the stored gas can be achieved when hydrates are dissociated. Hydrate dissociation can be achieved by a simple pressure reduction or very moderate heating of the hydrate. Essentially, the hydrate needs to be brought outside the three-phase equilibrium conditions.
- Hydrate formation/dissociation is an environmentally friendly process since the only by-product is  $\text{H}_2\text{O}$ . Promoters, when used, are usually at low concentrations. Furthermore, they can be completely miscible with  $\text{H}_2\text{O}$ , with low vapour pressure, which thus minimises promoter loss. This issue is important for both economic and environmental aspects.
- Hydrate formation is considered safe due to the low flammability risk and the non-explosive nature (due to the water presence) of the materials involved. Reduced risk (compared to liquefied natural gas or compressed natural gas) is also involved in the transportation of hydrate materials.

While initially there was significant excitement in the scientific community regarding the potential use of hydrates for gas storing materials, currently hydrates are short of meeting the US Department of Energy targets for gas-storage capacities of mobile applications (i.e. reasons for the particular shortfall include: (i) multiple occupancy in the small cages is not confirmed, and (ii) the tuning effect remains difficult to implement experimentally). Nevertheless, due to the number of significant advantages mentioned earlier, there is an increased interest from both academia and industry for hydrate gas-storage applications, focusing particularly on stationary applications, where the target storage capacities can be lowered.

### 3.5. Gas diffusivity studies

The use of MD simulations for the calculation of self-diffusion coefficients,  $D$ , is an attractive alternative to performing experimental measurements. The self-diffusion coefficient can be calculated using the Einstein relation, according to which  $D$  is obtained from the solute mean square displacement [19,20]:

$$D = \frac{1}{6} \lim_{t \rightarrow \infty} \frac{d}{dt} \frac{1}{N} \sum_{i=1}^N [\mathbf{r}_i(0) - \mathbf{r}_i(t)]^2, \quad (8)$$

where  $\mathbf{r}_i(t)$  is the unfolded position of the centre of mass of the solute at time  $t$ , and the angle brackets indicate an ensemble average over all solute molecules and time origins. To further improve the statistics of the MD results, the self-diffusion coefficient for each state point can be calculated by averaging the results of multiple independent simulations, each one starting from a different initial configuration, thus leading to a wide divergence of the trajectories of the molecules. Numerous MD studies can be found in the literature [130–138], that examine real fluids such as  $\text{H}_2$ ,  $\text{CO}_2$ ,  $\text{CH}_4$  and  $\text{H}_2\text{O}$  for a wide range of conditions.

The diffusion of hydrate-forming guests in the aqueous phase is an important process for hydrate formation since the guest molecules have to diffuse through liquid water in order to reach the hydrate–liquid interface, where hydrate formation occurs, and be enclathrated within the hydrate crystal structure. A series of MD simulations over a wide range of temperatures at 0.1 MPa were performed in order to calculate the self-diffusion coefficients of the first five  $n$ -alkanes in water at infinite dilution. Figure 14 (top-right panel), shows the self-diffusion coefficients of  $\text{CH}_4$ ,  $\text{C}_2\text{H}_6$ ,  $\text{C}_3\text{H}_8$ ,  $n\text{-C}_4\text{H}_{10}$  and  $n\text{-C}_5\text{H}_{12}$  in  $\text{H}_2\text{O}$  at 0.1 MPa, for the temperature range 274.9–333.15 K. In all cases, the self-diffusion coefficients increase with temperature, which is typical for gases dissolved in liquids. The MD-based simulations have been compared with available experimental data by Michalis et al. [32] in an effort to examine the accuracy of the predictions using the TIP4P/2005 [71] model for water

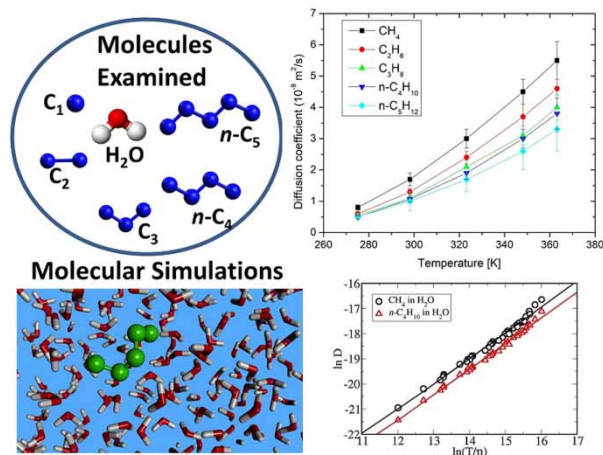


**Figure 14.** Schematic of the simulations of the diffusivities in the aqueous phase. Shown are the five molecules examined. The top-right panel shows the self-diffusion coefficient as a function of temperature at pressure 0.1 MPa (solid lines are guide to the eye only). The bottom-right panel shows the  $\ln(D)$  vs.  $\ln(T/\eta)$  for the case of  $\text{CH}_4$  (black circles) and  $n\text{-C}_4\text{H}_{10}$  (red triangles) diffusing in  $\text{H}_2\text{O}$ , where  $\eta$  is the solvent viscosity. The solid lines correspond to the best-fit lines.

and the TraPPE [139] force field for *n*-alkanes. It was concluded that the combination of TIP4P/2005 – TraPPE models provided an excellent agreement between the MD simulation results and the experiments for all the systems and conditions examined.

Subsequently, for the case of CH<sub>4</sub> and *n*-C<sub>4</sub>H<sub>10</sub>, MD simulations have been performed in a wide range of temperatures and for higher pressures up to 200 MPa. The MD-calculated self-diffusion coefficients were correlated using a Speedy–Angell-type [140] phenomenological equation that captures the pressure and temperature behaviour of the CH<sub>4</sub> and *n*-C<sub>4</sub>H<sub>10</sub> which can be used for engineering calculations. Furthermore, as the bottom-right panel of Figure 14 indicates, it was shown [32] that the self-diffusion coefficients CH<sub>4</sub> and *n*-C<sub>4</sub>H<sub>10</sub> obey the Stokes–Einstein equation [141]. In order to do so, one needs to examine the behaviour of the scaling law  $D \sim \left(\frac{T}{\eta}\right)^t$ , where  $D$  is the MD-calculated self-diffusion coefficient of the solute,  $T$  is the temperature,  $\eta$  is the MD-calculated viscosity of the solvent and  $t$  is a numerical exponent. By plotting  $D$  versus  $\left(\frac{T}{\eta}\right)$  in a logarithmic plot, the slope can be calculated which is equal to the exponent  $t$ . If the slope is equal to one, the classical Stokes–Einstein equation is obeyed. For any other value, the fractional Stokes–Einstein equation is obeyed [142,143]. Michalis et al. [32] reported for CH<sub>4</sub>, a value for  $t = 1.00 \pm 0.02$ , while for *n*-C<sub>4</sub>H<sub>10</sub>,  $t = 1.01 \pm 0.02$ . Both calculated slopes indicate that the classical Stokes–Einstein equation is satisfied.

#### 4. Conclusions

In the current work, we have demonstrated that performing studies at multiple length scales can be utilised efficiently in order to obtain properties essential to process design for clathrate hydrate systems. The applications in mind refer to gas-storage and gas separation. Hydrate properties that have been discussed include the three-phase equilibrium conditions, guest gas solubilities, structural parameters of the hydrate unit cell, cage occupancies and guest gas diffusivities in the aqueous phase. We have reported an overview of recent studies by our research group on molecular simulation, macroscopic computational and experimental studies of pure and mixed hydrates. The important conclusions of the previous works were also highlighted here.

#### Acknowledgments

This publication was made possible thanks to an NPRP award [NPRP 6–1547–2–632] from the Qatar National Research Fund (a member of The Qatar Foundation). The statements made herein are solely the responsibility of the authors. We

are grateful to the High Performance Computing Center of Texas A&M University at Qatar, and to the High Performance Computing Cluster of the Environmental Research Laboratory (NCSR ‘Demokritos’) for generous computational resource allocation.

#### Disclosure statement

No potential conflict of interest was reported by the authors.

#### ORCID

Ioannis N. Tsimpanogiannis  <http://orcid.org/0000-0002-3466-1873>

Vasileios K. Michalis  <http://orcid.org/0000-0003-3070-3949>

Othonas A. Moulton  <http://orcid.org/0000-0001-7477-9684>

Athanasios K. Stubos  <http://orcid.org/0000-0001-8449-1932>

Ioannis G. Economou  <http://orcid.org/0000-0002-2409-6831>

#### References

- [1] E.D. Sloan and C.A. Koh, *Clathrate Hydrates of Natural Gases*, 3rd ed. (Taylor & Francis, CRC Press, Boca Raton, FL, 2008).
- [2] S. Thomas and R.A. Dawe, *Energy*. **28**, 1461 (2003).
- [3] W.L. Mao, H.K. Mao, A.F. Goncharov, V.V. Struzhkin, Q. Guo, J. Hu, J. Shu, R.J. Hemley, M. Somayazulu, and Y. Zhao, *Science*. **297**, 2247 (2002).
- [4] H.P. Veluswamy, R. Kumar, and P. Linga, *Appl Energy*. **122**, 112 (2014).
- [5] P.G. Brewer, G. Friederich, E.T. Peltzer, and F.M. Orr Jr., *Science*. **284**, 943 (1999).
- [6] R. Boswell and T.S. Collett, *Energy Environ Sci*. **4**, 1206 (2010).
- [7] S.P. Kang and H. Lee, *Environ Sci Technol*. **34**, 4397 (2000).
- [8] Y.T. Seo, I.L. Moudrakovski, J.A. Ripmeester, J.-W. Lee, and H. Lee, *Environ Sci Technol*. **39**, 2315 (2005).
- [9] P. Linga, R. Kumar, and P. Englezos, *J Haz Materials*. **149**, 625 (2007).
- [10] A. Adeyemo, R. Kumar, P. Linga, J. Ripmeester, and P. Englezos, *Int J Greenhouse Gas Control*. **4**, 478 (2010).
- [11] P. Linga, N. Daraboina, J. Ripmeester, and P. Englezos, *Chem Eng Sci*. **68**, 617 (2012).
- [12] M. Van Denderen, E. Ineke, and M. Golombok, *Ind Eng Chem Res*. **48**, 5802 (2009).
- [13] N. Dabrowski, C. Windmeir, and L.R. Oelrich, *Energy Fuels*. **23**, 5603 (2009).
- [14] H. Kubota, K. Shimizu, Y. Tanaka, and T. Makita, *J Chem Eng Japan*. **17**, 423 (1984).
- [15] M.S. Rahman, M. Ahmed, and X.D. Chen, *Separ & Purif Rev*. **35**, 59 (2006).
- [16] K.-N. Park, S.Y. Hong, J.W. Lee, K.C. Kang, Y.C. Lee, M.-G. Ha, and J.D. Lee, *Desalination*. **274**, 91 (2011).
- [17] Y.T. Ngan and P. Englezos, *Ind Eng Chem Res*. **35**, 1894 (1996).
- [18] J. Ripmeester, *Ann N Y Acad Sci*. **912**, 1 (2000).
- [19] M.P. Allen and D.J. Tildesley, *Computer Simulation of Liquids* (Oxford University Press, New York, 1987).
- [20] D. Frenkel and B. Smit, *Understanding Molecular Simulation: From Algorithms to Applications*, 2nd ed. (Academic Press, San Diego, CA, 2002).

- [21] S. Succi, *The Lattice Boltzmann Equation for Fluid Dynamics and Beyond* (Oxford University Press, Oxford, 2001).
- [22] M.J. Blunt, B. Bijeljic, H. Dong, O. Gharbi, S. Iglauer, P. Mostaghimi, A. Paluszny, and C. Pentland, *Adv Water Resour.* **51**, 197 (2013).
- [23] I.N. Tsimpanogiannis and P.C. Lichtner, *J Phys Chem C.* **117**, 11104 (2013).
- [24] P.J. Hoogerbrugge and J.M.V.A. Koelman, *Europhys Lett.* **19**, 155 (1992).
- [25] R.D. Groot and P.B. Warren, *J Chem Phys.* **107**, 4423 (1997).
- [26] K. Aziz and A. Settari, *Petroleum Reservoir Simulation* (Applied Science Publishers, New York, NY, 1979).
- [27] V.K. Michalis, J. Costandy, I.N. Tsimpanogiannis, A.K. Stubos, and I.G. Economou, *J Chem Phys.* **142**, 044501 (2015).
- [28] J. Costandy, V.K. Michalis, I.N. Tsimpanogiannis, A.K. Stubos, and I.G. Economou, *J Chem Phys.* **143**, 094506 (2015).
- [29] V.K. Michalis, I.N. Tsimpanogiannis, A.K. Stubos, and I.G. Economou, *Phys Chem Chem Phys* **18**, 23538 (2016).
- [30] J. Costandy, V.K. Michalis, I.N. Tsimpanogiannis, A.K. Stubos, and I.G. Economou, *Mol Phys.* **114**, 2672 (2016).
- [31] J. Costandy, V.K. Michalis, I.N. Tsimpanogiannis, A.K. Stubos, and I.G. Economou, *J Chem Phys.* **144**, 124512 (2016).
- [32] V.K. Michalis, O.A. Moulτος, I.N. Tsimpanogiannis, and I.G. Economou, *Fluid Phase Equilib.* **407**, 236 (2016).
- [33] N.I. Papadimitriou, I.N. Tsimpanogiannis, I.G. Economou, and A.K. Stubos, *Mol Phys.* **112**, 2258 (2014).
- [34] N.I. Papadimitriou, I.N. Tsimpanogiannis, I.G. Economou, and A.K. Stubos, *J Phys Conf Series.* **640**, 012026 (2015).
- [35] N.I. Papadimitriou, I.N. Tsimpanogiannis, I.G. Economou, and A.K. Stubos, *J Chem Eng Data.* **61**, 2886 (2016).
- [36] N.I. Papadimitriou, I.N. Tsimpanogiannis, I.G. Economou, and A.K. Stubos, *Mol Phys.* **114**, 2664 (2016).
- [37] N.I. Papadimitriou, I.N. Tsimpanogiannis, I.G. Economou, and A.K. Stubos, *Mol Phys.* **115**, 1274 (2017).
- [38] N.I. Papadimitriou, I.N. Tsimpanogiannis, I.G. Economou, and A.K. Stubos, *J Chem Thermodynamics.* **117**, 128 (2018).
- [39] N.I. Papadimitriou, I.N. Tsimpanogiannis, I.G. Economou, and A.K. Stubos, *Monte Carlo Simulations of the Separation of a Binary Gas Mixture (CH<sub>4</sub> + CO<sub>2</sub>) using Hydrates*, 2018 (Submitted).
- [40] I.N. Tsimpanogiannis and I.G. Economou, *J Supercrit Fluids.* **134**, 51 (2018).
- [41] I.N. Tsimpanogiannis, I.G. Economou, and A.K. Stubos, *Fluid Phase Equilib.* **371**, 106 (2014).
- [42] I.N. Tsimpanogiannis, N.I. Diamantonis, I.G. Economou, N.I. Papadimitriou, and A.K. Stubos, *Chem Eng Res Des.* **92**, 2992 (2014).
- [43] I.N. Tsimpanogiannis, D. Thomas, I.G. Economou, and A.K. Stubos, "Evaluation of a Simple Model for Hydrate Equilibrium Calculations of Binary Gas Hydrates with Application to Gas-Mixture Separation," Paper presented at the 8th International Conference on Gas Hydrates, Beijing, July 28–August 1, 2014.
- [44] S. El Meragawi, N.I. Diamantonis, I.N. Tsimpanogiannis, and I.G. Economou, *Fluid Phase Equilib.* **413**, 209 (2016).
- [45] P. Kastanidis, G.E. Romanos, V.K. Michalis, I.G. Economou, A.K. Stubos, and I.N. Tsimpanogiannis, *Fluid Phase Equilib.* **424**, 152 (2016).
- [46] P. Kastanidis, G.E. Romanos, A.K. Stubos, I.G. Economou, and I.N. Tsimpanogiannis, *Fluid Phase Equilib.* **451**, 96 (2017).
- [47] P. Kastanidis, V.K. Michalis, G.E. Romanos . . . I.N. Tsimpanogiannis, *J Chem Eng Data* **63**, 1027 (2018). Solubility of Methane and Carbon Dioxide in the Aqueous Phase of the Ternary (Methane + Carbon Dioxide + Water) Mixture: Experimental Measurements and Molecular Dynamics Simulations. doi:10.1021/acs.jced.7b00777
- [48] A.J.C. Ladd and L.V. Woodcock, *Chem Phys Lett.* **51**, 155 (1977).
- [49] E.K. Karakatsani and I.G. Economou, *J Phys Chem B.* **110**, 9252 (2006).
- [50] N.I. Diamantonis and I.G. Economou, *Energy Fuels.* **25**, 3334 (2011).
- [51] D.Y. Peng and D.B. Robinson, *Ind Eng Chem Fundam.* **15**, 59 (1976).
- [52] G. Soave, *Chem Eng Sci.* **27**, 1197 (1972).
- [53] J.H. Van der Waals and J.C. Platteeuw, *Adv Chem Phys.* **2**, 1 (1959).
- [54] T.J. Frankcombe and G.-J. Kroes, *Phys Chem Chem Phys.* **13**, 13410 (2011).
- [55] S. Circone, S.H. Kirby, L.A. Stern, *J Phys Chem B.* **109**, 9468 (2015).
- [56] T.C. Hansen, A. Falenty, W.F. Kuhs, *J Chem Phys.* **144**, 054301 (2016).
- [57] J. Qin, W.F. Kuhs, *AIChE J.* **59**, 2155 (2013).
- [58] V.V. Sizov and E.M. Piotrovskaya, *J Phys Chem B.* **111**, 2886 (2007).
- [59] N.I. Papadimitriou, I.N. Tsimpanogiannis, A.K. Stubos, A. Martin, L.J. Rovetto, and C.J. Peters, *J Phys Chem Lett.* **1**, 1014 (2010).
- [60] M. Lasich, A. H. Mohammadi, K. Bolton, J. Vrabec, and D. Ramjugernath, *Fluid Phase Equilib.* **369**, 47 (2014).
- [61] H. Henley and A. Lucia, *J Nat Gas Sci Eng.* **26**, 446 (2015).
- [62] A. Martin and C.J. Peters, *J Phys Chem B.* **113**, 7558 (2009).
- [63] G.M. Kontogeorgis and I.G. Economou, *J Supercrit Fluids.* **55**, 421 (2010).
- [64] D. van der Spoel, E. Lindahl, B. Hess, G. Groenhof, A.E. Mark, and H.J.C. Berendsen, *J Comput Chem.* **26**, 1701 (2005).
- [65] B. Hess, C. Kutzner, D. van der Spoel, and E. Lindahl, *J Chem Theory Comput.* **4**, 435 (2008).
- [66] S. Pronk, S. Pall, P. Larsson, P. Bjelkmar, R. Apostolov, M.R. Shirts, J.C. Smith, P.M. Kasson, D. van der Spoel, B. Hess, and E. Lindahl, *Bioinformatics.* **29**, 845 (2013).
- [67] M. Martin, *Mol Simul.* **39**, 1212 (2013).
- [68] G. Guerin, D. Goldberg, and A. Meltser, *J Geophys Res.* **104B**, 17781 (1999).
- [69] M.B. Helgerud, J. Dvorkin, A. Nur, A. Sakai, and T. Collett, *Geophys Res Lett.* **26**, 2021 (1999).
- [70] J.L.F. Abascal, F. Sanz, R.G. Fernandez, and C. Vega, *J Chem Phys.* **122**, 234511 (2005).



- [71] J.L.F. Abascal and C. Vega, *J Chem Phys.* **123**, 234505 (2005).
- [72] M.M. Conde, C. Vega, C. McBride, E.G. Noya, R. Ramirez, and L.M. Sese, *J Chem Phys.* **132**, 114503 (2010).
- [73] C. McBride, C. Vega, E.G. Noya, R. Ramirez, and L.M. Sese, *J Chem Phys.* **131**, 024506 (2009).
- [74] B. Fang, F. Ning, P. Cao, L. Peng, J. Wu, Z. Zhang, T.J.H. Vlught, and S. Kjelstrup, *J Phys Chem B.* **121**, 2179 (2017).
- [75] R. García Fernández, J.L.F. Abascal, and C. Vega, *J Chem Phys.* **124**, 144506 (2006).
- [76] M.M. Conde and C. Vega, *J Chem Phys.* **138**, 056101 (2013).
- [77] J.M. Miguez, M.M. Conde, J.-P. Torre, F.J. Blas, M.M. Pineiro, and C. Vega, *J Chem Phys.* **142**, 124505 (2015).
- [78] T. Yagasaki, M. Matsumoto, and H. Tanaka, *J Phys Chem C.* **120**, 21512 (2016).
- [79] W.L. Jorgensen, J.D. Madura, and C.J. Swenson, *J Am Chem Soc.* **106**, 6638 (1984).
- [80] H. Docherty, A. Galindo, C. Vega, and E. Sanz, *J Chem Phys.* **125**, 074510 (2006).
- [81] J.J. Potoff and J.I. Siepmann, *AIChE J.* **47**, 1676 (2001).
- [82] M.H. Waage, T.J.H. Vlught, and S. Kjelstrup, *J Phys Chem B.* **121**, 7336 (2017).
- [83] Y.T. Tung, L.J. Chen, Y.P. Chen, and S.T. Lin, *J Phys Chem B.* **114**, 10804 (2010).
- [84] Y.T. Tung, L.J. Chen, Y.P. Chen, and S.T. Lin, *J Phys Chem C.* **115**, 7504 (2011).
- [85] Y.-T. Tung, L.-J. Chen, Y.-P. Chen, and S.-T. Lin, *J Phys Chem B.* **115**, 15295 (2011).
- [86] G.S. Smirnov and V.V. Stegailov, *J Chem Phys.* **136**, 044523 (2012).
- [87] D.P. Luis, I.E. Romero-Ramirez, A. Gonzalez-Calderon, and J. Lopez-Lemus, *J Chem Phys.* **148**, 114503 (2018).
- [88] W.R. Parrish and J.M. Prausnitz, *Ind Eng Chem Proc Des Dev.* **11**, 26 (1972).
- [89] G.D. Holder, G. Corbin, and K.D. Papadopoulos, *Ind Eng Chem Fund.* **19**, 282 (1980).
- [90] R. Sun and Z. Duan, *Chem Geol.* **244**, 248 (2007).
- [91] J.B. Klauda and S.I. Sandler, *Ind Eng Chem Res.* **39**, 3377 (2000).
- [92] J.B. Klauda and S.I. Sandler, *Chem Eng Sci.* **58**, 27 (2002).
- [93] A.L. Ballard and E.D. Sloan, *Fluid Phase Equilib.* **194–197**, 371 (2002).
- [94] A.L. Ballard, E.D. Sloan, *Fluid Phase Equilib.* **218**, 15 (2004).
- [95] H. Tanaka, T. Nakatsuka, and K. Koga, *J Chem Phys.* **121**, 5488 (2004).
- [96] K. Katsumasa, K. Koga, and H. Tanaka, *J Chem Phys.* **127**, 044509 (2007).
- [97] A. Martin, *J Phys Chem B.* **114**, 9602 (2010).
- [98] M.-J. Hwang, G.D. Holder, and S.R. Zele, *Fluid Phase Equilib.* **83**, 437 (1993).
- [99] S.R. Zele, S.-Y. Lee, and G.D. Holder, *J Phys Chem B.* **103**, 10250 (1999).
- [100] A. Martin and C.J. Peters, *J Phys Chem C.* **113**, 422 (2009).
- [101] V.T. John and G.D. Holder, *J Phys Chem.* **85**, 1811 (1981).
- [102] V.T. John and G.D. Holder, *J Phys Chem.* **86**, 455 (1982).
- [103] V.T. John and G.D. Holder, *J Phys Chem.* **89**, 3279 (1985).
- [104] K.A. Sparks, J.W. Tester, Z. Cao, and B.L. Trout, *J Phys Chem B.* **103**, 6300 (1999).
- [105] R.J. Bakker, J. Dubessy, M. Cathelineau, *Geochim Cosmochim Acta.* **60**, 1657 (1996).
- [106] R.J. Bakker, In *Gas Hydrates: Relevance to World Margin Stability and Climate Change*, edited by J.-P. Henriot and J. Mienert (Geological Society, London, 1998), Special Publications, Vol. **137**, p. 75.
- [107] G.D. Holder, S.P. Zetts, and N. Pradhan, *Rev Chem Eng.* **5**, 1 (1988).
- [108] G.D. Holder, S.T. Malekar, and E.D. Sloan, *Ind Eng Chem Fund.* **23**, 123 (1984).
- [109] M.N. Khan, P. Warriar, C.J. Peters, and C.A. Koh, *Fluid Phase Equilib.* **463**, 48 (2018).
- [110] S.Z.S. Al Ghafri, E. Forte, G.C. Maitland, J.J. Rodriguez-Henriquez, and J.P.M. Trusler, *J Phys Chem B.* **118**, 14461 (2014).
- [111] J. Qin, R.J. Rosenbauer, and Z. Duan, *J Chem Eng Data.* **53**, 1246 (2008).
- [112] S.C. Velaga, J.S. Levine, R.P. Warzinski, and B.J. Anderson, *Fluid Phase Equilib.* **414**, 75 (2016).
- [113] T. Huang, C. Li, W. Jia, and Y. Peng, *Fluid Phase Equilib.* **427**, 35 (2016).
- [114] Z. Duan, R. Sun, C. Zhu, and I.M. Chou, *Mar Chem.* **98**, 131 (2006).
- [115] B. Widom, *J Chem Phys.* **39**, 2808 (1963).
- [116] H.J.C. Berendsen, J.R. Grigera, and T.P. Straatsma, *J Phys Chem.* **91**, 6269 (1987).
- [117] I.F. Silvera and V.V. Goldman, *J Chem Phys.* **69**, 4209 (1978).
- [118] H. Lee, J.-W. Lee, D.Y. Kim, J. Park, Y.-T. Seo, H. Zeng, I.L. Moudrakovski, C.I. Ratcliffe, and J.A. Ripmeester, *Nature.* **434**, 743 (2005).
- [119] D.-Y. Kim, J. Park, J.-W. Lee, J.A. Ripmeester, and H. Lee, *J Am Chem Soc.* **128**, 15360 (2006).
- [120] R. Susilo, S. Alavi, J. Ripmeester, and P. Englezos, *Fluid Phase Equilib.* **263**, 6 (2008).
- [121] T. Sugahara, J.C. Haag, P.S.R. Prasad, A.A. Warntjes, E.D. Sloan, A.K. Sum, and C.A. Koh, *J Am Chem Soc.* **131**, 14616 (2009).
- [122] V.R. Avula, R.L. Gardas, and J.S. Sangwai, *J Nat Gas Sci Eng.* **33**, 509 (2016).
- [123] H.P. Veluswamy, S. Kumar, R. Kumar, P. Rangsunvigit, and P. Linga, *Fuel.* **182**, 907 (2016).
- [124] D.-Y. Koh, H. Kang, J. Jeon, Y.-H. Ahn, Y. Park, H. Kim, and H. Lee, *J Phys Chem C.* **118**, 3324 (2014).
- [125] <http://php.net/>
- [126] <https://developers.google.com/chart/interactive/docs/index>
- [127] <http://www.w3.org/html/>
- [128] [http://www.onlamp.com/pub/a/php/2001/05/03/php\\_foundations.html](http://www.onlamp.com/pub/a/php/2001/05/03/php_foundations.html)
- [129] H.P. Veluswamy, A. Kumar, Y. Seo, J.D. Lee, and P. Linga, *Appl Energy.* **216**, 262 (2018).
- [130] D.M. Heyes, M.J. Cass, J.G. Powles, and W.A.B. Evans, *J Phys Chem B.* **111**, 1455 (2007).
- [131] D. Zabala, C. Nieto-Draghi, J.C. de Hemptinne, and A.L. López de Ramos, *J Phys Chem B.* **112**, 16610 (2008).
- [132] R.E. Zeebe, *Geochim Cosmochim Acta.* **75**, 2483 (2011).
- [133] Z. Makrodimitri, D.J.M. Unruh, and I.G. Economou, *J Phys Chem B.* **115**, 1429 (2011).



- [134] G. Raabe and R.J. Sadus, *J Chem Phys.* **137**, 104512 (2012).
- [135] O.A. Moulτος, I.N. Tsimpanogiannis, A.Z. Panagiotopoulos, and I.G. Economou, *J Phys Chem B.* **118**, 5532 (2014).
- [136] C.G. Aimoli, E.J. Maginn, and C.R.A. Abreu, *J Chem. Phys.* **141**, 134101 (2014).
- [137] G. Kikugawa, S. Ando, J. Suzuki, Y. Naruke, T. Nakano, and T. Ohara, *J Chem Phys.* **142**, 24503 (2015).
- [138] O.A. Moulτος, I.N. Tsimpanogiannis, A.Z. Panagiotopoulos, and I.G. Economou, *J Chem Thermodyn.* **93**, 424 (2016).
- [139] M.G. Martin and J.I. Siepmann, *J Phys Chem B.* **102**, 2569 (1998).
- [140] R.J. Speedy and C.A. Angell, *J Chem Phys.* **65**, 851 (1976).
- [141] E.L. Cussler, *Diffusion: Mass Transfer in Fluid Systems*, 3rd ed Cambridge University Press, Cambridge, 2009
- [142] L. Xu, F. Mallamace, Z. Yan, F.W. Starr, S.V. Buldyrev, and E.H. Stanley, *Nature Phys.* **5**, 565 (2009).
- [143] K.R. Harris, *J Chem Phys.* **131**, 054503 (2009).
- [144] Z.H. Duan and S.D. Mao, *Geochim Cosmochim Acta.* **70**, 3369 (2006).